ESC European Society of Cardiology

Cardiovascular Research (2023) **119**, 2697–2711
https://doi.org/10.1093/cvr/cvad138

PDE4D mediates impaired β-adrenergic receptor signalling in the sinoatrial node in mice with hypertensive heart disease

Tristan W. Dorey, Megan D. McRae, Darrell D. Belke, and Robert A. Rose *

Libin Cardiovascular Institute, Department of Cardiac Sciences, Department of Physiology and Pharmacology, Cumming School of Medicine, University of Calgary, 3280 Hospital Drive NW, Calgary, AB, T2N 4Z6, Canada

Received 17 December 2022; revised 6 June 2023; accepted 18 July 2023; online publish-ahead-of-print 29 August 2023

Time of primary review: 49 days

Aims The sympathetic nervous system increases HR by activating β-adrenergic receptors (β-ARs) and increasing cAMP in sinoatrial node (SAN) myocytes while phosphodiesterases (PDEs) degrade cAMP. Chronotropic incompetence, the inability to regulate heart rate (HR) in response to sympathetic nervous system activation, is common in hypertensive heart disease; however, the basis for this is poorly understood. The objective of this study was to determine the mechanisms leading to chronotropic incompetence in mice with angiotensin II (AngII)-induced hypertensive heart disease.

Methods and results C57BL/6 mice were infused with saline or AngII (2.5 mg/kg/day for 3 weeks) to induce hypertensive heart disease. HR and SAN function in response to the β-AR agonist isoproterenol (ISO) were studied *in vivo* using telemetry and electrocardiography, in isolated atrial preparations using optical mapping, in isolated SAN myocytes using patch-clamping, and using molecular biology. AngII-infused mice had smaller increases in HR in response to physical activity and during acute ISO injection. Optical mapping of the SAN in AngII-infused mice demonstrated impaired increases in conduction velocity and altered conduction patterns in response to ISO. Spontaneous AP firing responses to ISO in isolated SAN myocytes from AngII-infused mice were impaired due to smaller increases in diastolic depolarization (DD) slope, hyperpolarization-activated current (I_f), and L-type Ca^{2+} current ($I_{Ca,L}$). These changes were due to increased localization of PDE4D surrounding β_1- and β_2-ARs in the SAN, increased SAN PDE4 activity, and reduced cAMP generation in response to ISO. Knockdown of PDE4D using a virus-delivered shRNA or inhibition of PDE4 with rolipram normalized SAN sensitivity to β-AR stimulation in AngII-infused mice.

Conclusions AngII-induced hypertensive heart disease results in impaired HR responses to β-AR stimulation due to up-regulation of PDE4D and reduced effects of cAMP on spontaneous AP firing in SAN myocytes.

* Corresponding author. Tel: 403 210 3922, E-mail: robert.rose@ucalgary.ca

Graphical Abstract

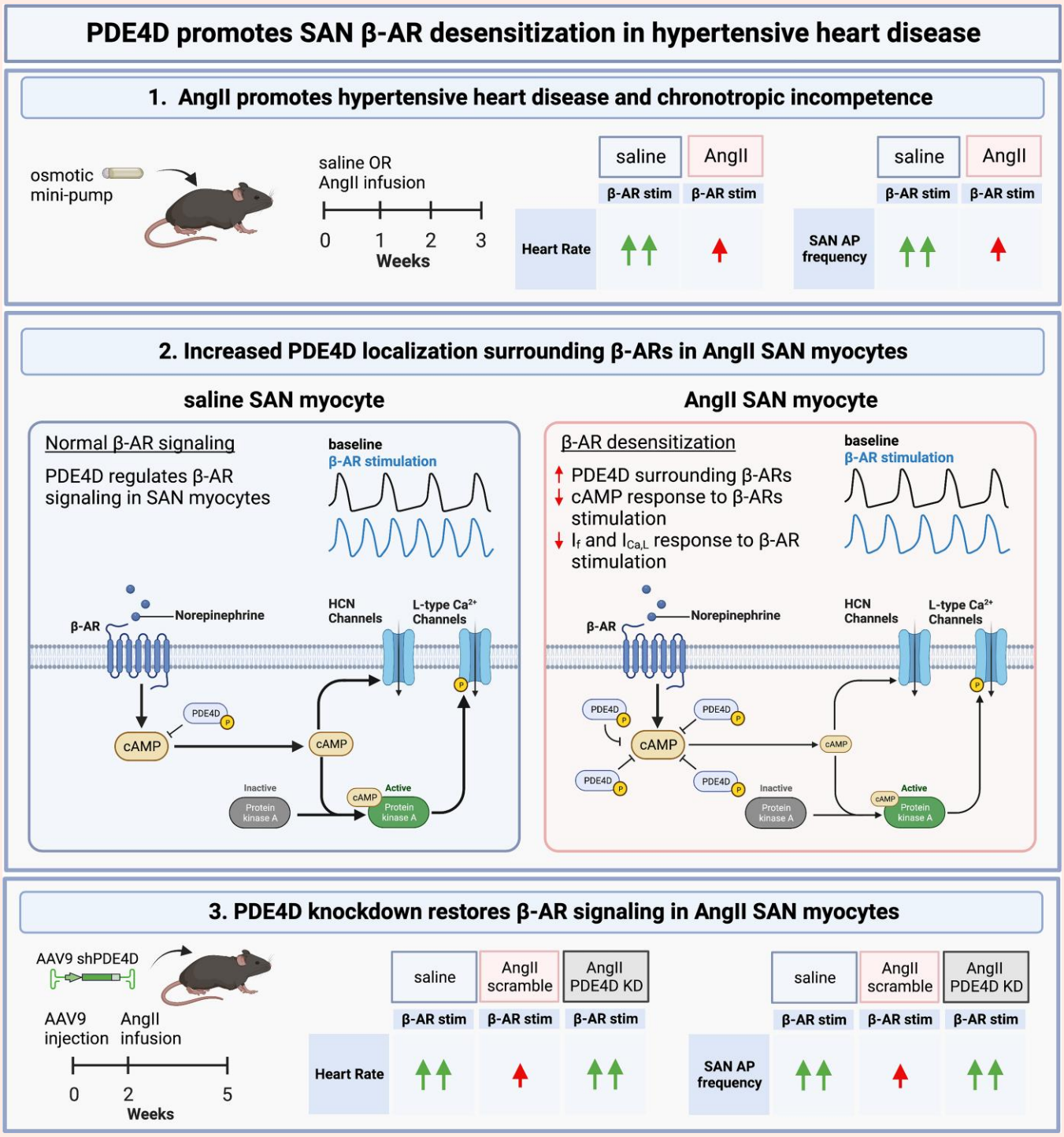

Keywords Chronotropic incompetence • Sinoatrial node • Heart rate • β-Adrenergic receptors • Phosphodiesterase • Ion channels

1. Introduction

Hypertension is the most common form of cardiovascular disease[1] and is the number one risk factor for the development of heart failure.[2,3] Hypertension increases myocardial work resulting in elevated sympathetic nervous system outflow to the heart as well as structural and electrical remodelling of the myocardium.[4] Heart rate (HR) is a critical regulator of cardiac performance that is controlled by the intrinsic properties of the sinoatrial node (SAN) and its modulation by the autonomic nervous system (ANS).[5,6] Impaired HR regulation in response to physical activity or

stress, denoted chronotropic incompetence, is common in the setting of hypertensive heart disease and heart failure and is associated with increased mortality.[7–9]

Increases in HR occur predominantly through sympathetic postganglionic release of norepinephrine onto SAN myocytes. Norepinephrine binds to β_1- and β_2-adrenergic receptors (ARs) on SAN myocytes, which activate adenylyl cyclase and increase cyclic adenosine monophosphate (cAMP) production.[5,6] A rise in intracellular cAMP elicits a positive shift in steady-state activation of the hyperpolarization-activated current (I_f) by direct binding of cAMP to hyperpolarization-activated cyclic nucleotide gated (HCN) channels. This results in larger inward current during the start of diastolic depolarization (DD) and an increase in SAN spontaneous action potential (AP) firing frequency.[6] Additionally, cAMP increases SAN myocyte AP firing via cAMP-mediated activation of protein kinase A (PKA) and subsequent increases in L-type Ca^{2+} current ($I_{Ca,L}$; carried by Cav1.2 and Cav1.3) and effects on sarcoplasmic reticulum (SR) Ca^{2+}-handling proteins that determine Ca^{2+} transient (CaT) morphology.[5,6,10] Membrane currents and SR Ca^{2+} handling represent a coupled system controlling diastolic depolarization in SAN myocytes.[10]

Phosphodiesterases (PDEs) are critical regulators of cAMP signalling in the SAN[11,12] and have been shown to blunt cardiac β-AR signalling.[13] PDE3 and PDE4 are major contributors to total PDE activity in the SAN and potently regulate SAN function.[11,12,14] The PDE4 family accounts for ~60% of total cardiac PDE activity in rodent hearts.[12,13,15] Furthermore, the PDE4D isoform predominantly regulates β-AR-induced cAMP signalling in the heart and is well conserved between rodent and human cardiomyocytes.[13,16–19]

Recent studies have demonstrated that chronotropic incompetence in the setting of human and animal models of hypertensive heart disease and heart failure result from SAN dysfunction, a blunting of maximum HR, as well as direct β-AR desensitization of the SAN.[20–22] Consistent with this, our lab has demonstrated that mice infused with the vasoconstrictor angiotensin II (AngII) have overt hypertensive heart disease, SAN dysfunction, and reduced responsiveness of the SAN to β-AR stimulation.[23,24] Despite these findings, the mechanisms responsible for β-AR desensitization of the SAN in hypertensive heart disease are still unknown. As such, the aim of the present study was to directly assess HR and SAN function in response to β-AR stimulation in mice with AngII-induced hypertensive heart disease. We show that AngII promotes progressive chronotropic incompetence due to impaired β-AR regulation of spontaneous AP firing in SAN myocytes and that PDE4D plays a major role in this process.

2. Methods

2.1 Experimental techniques

This study used male wildtype C57Bl/6 mice between the ages of 13 and 16 weeks. Mice were infused with saline or AngII (2.5 mg/kg/day) for 3 weeks using osmotic minipumps (Alzet, Cupertino, CA). Cardiac structure was assessed by echocardiography.[24,25] HR and SAN function were assessed using telemetry in awake and freely moving mice as well as electrocardiography in anaesthetized mice.[23,25] SAN function and conduction patterns were assessed using high-resolution optical mapping in isolated atrial preparations.[24–26] Spontaneous AP morphology and ionic currents (I_f, $I_{Ca,L}$) were investigated using patch-clamping in isolated SAN myocytes.[24,25] Ca^{2+} transient morphology was measured using Ca^{2+} imaging in isolated SAN myocytes. cAMP levels and PDE activity were assessed using commercially available kits.[25] SAN mRNA abundance and protein levels were investigated using qPCR and western blotting.[24,25] Co-localization of PDE4D and β-ARs was assessed using immunocytochemistry. In some cases, mice were injected retro-orbitally with a custom made adeno-associated virus stereotype-9 (AAV9; 1.5×10^{11} genomic copies/mouse) encoding an shRNA for murine PDE4D (or scrambled control) under the control of the U6 promoter (Vector Biolabs, Malvern, PA). Mice were used experimentally 5 weeks after virus injection. When combined with AngII infusion, AngII pumps were implanted two weeks after virus injection. For surgeries and tissue isolations, mice were anaesthetized using isoflurane (2%, inhalation). Mice were euthanized by cervical dislocation under isoflurane anaesthesia. Details for these approaches are available in the Data Supplement.

All experimental procedures were approved by the University of Calgary Animal Care and Use Committee and were in accordance with the guidelines of the Canadian Council on Animal Care and the NIH guide for the care and use of laboratory animals.

2.2 Statistics

All data are presented as means ± S.E.M. Statistical analysis was conducted using Prism version 9 (GraphPad Software). Normality of the data was assessed by Shapiro–Wilk test. Normally distributed data were analysed using Student's *t*-test, two-way analysis of variance (ANOVA) with a Holm-Sidak *post hoc* test, or two-way repeated measures ANOVA with a Holm-Sidak *post hoc* test as indicated in the figure legends. Non-parametric tests were used when data were not normally distributed. For cellular experiments, hierarchical statistical analyses were used to account for non-independent sampling (i.e. differences in the number of cells obtained from each animal). Statistical tests are reported in each figure legend, and differences are reported as $*P < 0.05$, $**P < 0.01$, $***P < 0.001$, or $****P < 0.0001$.

3. Results

3.1 Chronic AngII promotes chronotropic incompetence and β-AR desensitization *in vivo*

As expected,[24,27,28] three weeks of AngII infusion increased systolic and diastolic blood pressure (see Supplementary material online, *Figure S1A*) and resulted in cardiac hypertrophy as evident by increases in heart weight/tibia length (see Supplementary material online, *Figure S1B and C*). Echocardiography further demonstrates the occurrence of ventricular hypertrophy as indicated by increases in left ventricular anterior and posterior wall thickness, as well as reductions in left ventricular internal diameter, after 3 weeks of AngII infusion (see Supplementary material online, *Table S1*). Right and left atrial area was also increased after 3 weeks of AngII (see Supplementary material online, *Table S1*).

HR was monitored by telemetry in conscious mice during AngII (or saline) infusion (see Supplementary material online, *Figure S2*). Activity increased over three weeks of saline and AngII infusion with no differences between these groups (see Supplementary material online, *Figure S2A*). Conversely, increases in HR in association with increasing activity were reduced in AngII-infused mice (see Supplementary material online, *Figure S2B and C*). Intrinsic HR, measured during acute weekly injections of the ANS blockers atropine (10 mg/kg) and propranolol (10 mg/kg), also progressively declined during AngII infusion (see Supplementary material online, *Figure S2D*). At the end of three weeks of AngII infusion, HR decreased during high activity compared to saline-infused mice with no differences in activity levels between groups (see Supplementary material online, *Figure S2E and F*). Furthermore, heart rate variability (HRV; a surrogate measure of ANS activity), as assessed by the standard deviation of RR-intervals (SDNN) and root mean squared of the successive differences in RR-interval (RMSSD), was reduced during low and high activity in AngII-infused mice (see Supplementary material online, *Figure S2G and H*).

To directly assess HR responses to β-AR stimulation, mice were acutely injected with the β-AR agonist isoproterenol (ISO; 10 mg/kg). ISO rapidly increased HR in both saline- and AngII-infused mice (*Figure 1A and B*); however, peak HR responses to ISO were smaller in AngII-infused mice compared to saline-infused controls (*Figure 1C and D*). Collectively, these data demonstrate that AngII-infused mice exhibit SAN dysfunction and an impaired ability to increase HR in response to sympathetic nervous system activation and β-AR stimulation.

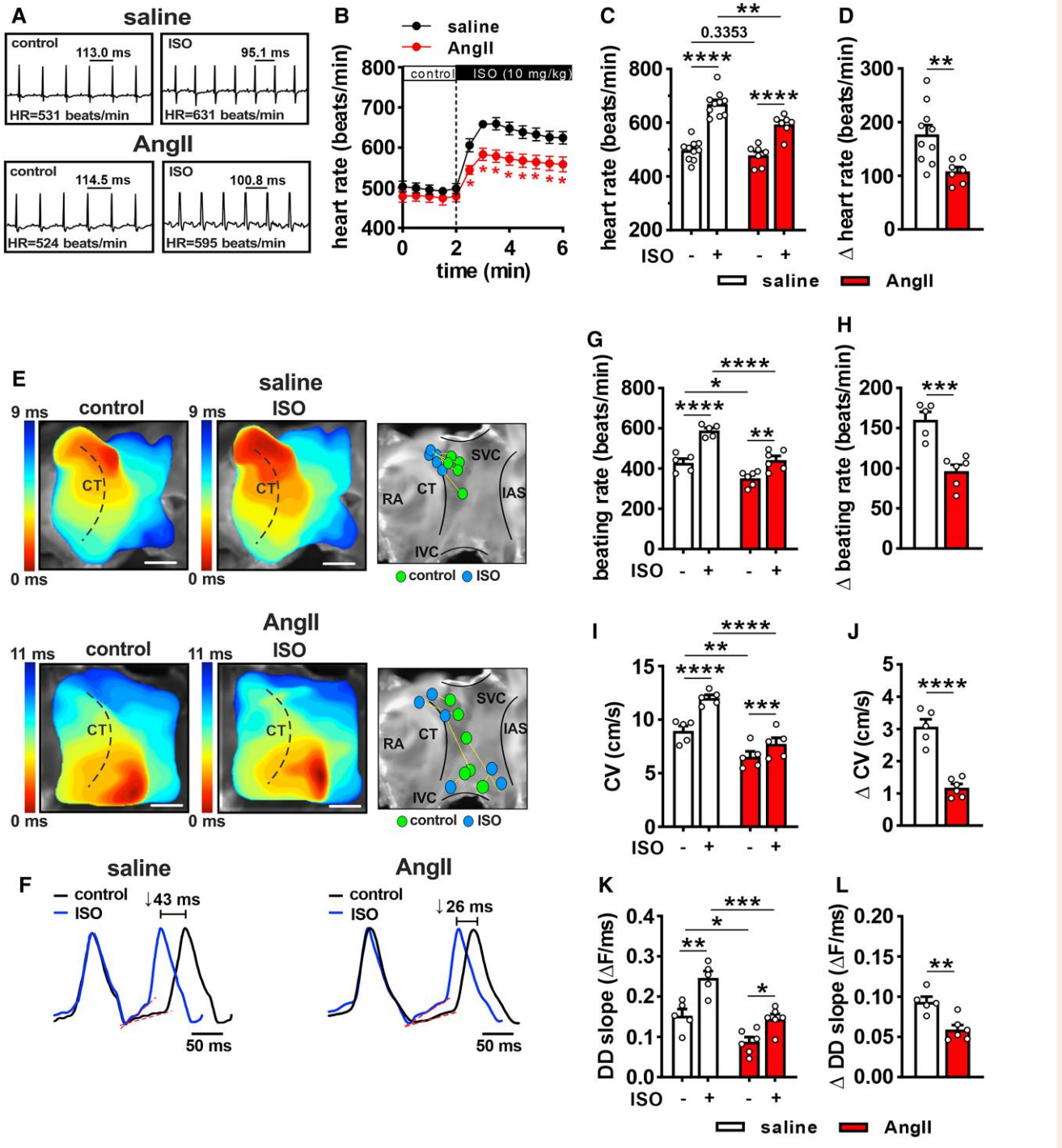

Figure 1 Chronotropic incompetence and impaired SAN electrical conduction in mice with AngII-induced hypertensive heart disease. (*A*) Representative ECG recordings in anaesthetized saline- and AngII-infused mice in control conditions and following acute intraperitoneal injection of isoproterenol (ISO; 10 mg/kg). (*B–D*) Summary of HR over time following ISO injection (*B*), average resting and peak HR responses to ISO (*C*) and change (Δ) in HR after ISO injection (*D*) in anaesthetized saline ($n = 10$) and AngII-infused ($n = 7$) mice. Data in panels *B* and *C* analysed by two-way repeated measures ANOVA with Holm-Sidak *post hoc* test. Data in panel *D* analysed by Student's *t*-test. (*E*) Representative activation maps and initial activation sites in isolated atrial preparations from saline- and AngII-infused mice in control condition and after superfusion of ISO (10 nM). Dashed lines indicate the crista terminalis (CT). Scale bar = 2 mm. RA, right atrium; SVC, superior vena cava; IVC, inferior vena cava; IAS, interatrial septum. (*F*) Optical action potentials (OAPs) from the SAN region of the right atrial posterior wall for saline- and AngII-infused mice before and after ISO. Red lines represent linear fitting of diastolic depolarization (DD) slope. (*G–L*) Summary data and Δ values for atrial preparation beating rate (G and *H*), conduction velocity (CV; *I* and *J*), and OAP DD slope (*K* and *L*) from saline ($n = 5$) and AngII ($n = 6$) atrial preparations before and after application of ISO. Data in panels *G*, *I*, and *K* analysed by two-way repeated measures ANOVA with Holm-Sidak *post hoc* test. Data in panels *H*, *J*, and *L* analysed by Student's *t*-test.

3.2 SAN electrical conduction and β-AR responsiveness are impaired in AngII-infused hearts

To investigate the basis for impaired HR responses to β-AR stimulation in AngII-infused mice, SAN electrical activation and conduction responses to ISO were investigated using high-resolution optical mapping in isolated atrial preparations. Activation maps of the right atrial posterior wall adjacent to the crista terminalis (*Figure 1E*) were used to quantify the location of the initial activation site within the SAN as well as local conduction velocity (CV) in control conditions and after application of ISO (10 nM). As expected, ISO shifted the initial activation site superiorly in saline hearts[29,30] (*Figure 1E*). In contrast, initial activation sites were highly variable in control conditions and displayed irregular shifts in the presence of ISO in AngII-infused hearts (*Figure 1E*). Furthermore, there was an increase in the occurrence of abnormal rhythms such as sinus pauses and rapid ectopic firing in atrial preparations from AngII-infused mice after ISO infusion (see Supplementary material online, *Figure S3*).

Optical APs recorded from the SAN region of the right atrial posterior wall show that the diastolic period between successive APs shortened in response to ISO but this effect was smaller in hearts from AngII-infused mice (*Figure 1F*). Consistent with this, as well as the reduced intrinsic rate and impaired β-AR responsiveness seen *in vivo*, atrial preparations from AngII-infused mice demonstrated lower intrinsic beating rates and reduced responsiveness to ISO compared to saline-infused controls (*Figure 1G* and *H*).

Local CV in the SAN region of the right atrial posterior wall was lower in AngII-infused mice compared to saline-infused mice in control conditions (*Figure 1I*). ISO increased CV in both groups; however, AngII-infused mice had diminished responses to ISO compared to saline-infused controls (*Figure 1I* and *J*). Optical action potentials (OAPs) were also analysed to quantify changes in DD slope in control conditions and in response to ISO (*Figure 1K* and *L*). In control conditions, DD slope was reduced in AngII-infused mice (*Figure 1K*). ISO increased DD slope in both groups; however, these effects were smaller in AngII-infused hearts (*Figure 1L*).

3.3 AngII impairs β-AR regulation of SAN myocyte electrophysiology

To further assess the mechanisms for β-AR desensitization in the SAN of AngII-infused mice, the effects of ISO on spontaneous APs in isolated SAN myocytes were measured (*Figure 2*). Consistent with the reduced intrinsic rates and decreased β-AR responsiveness observed *in vivo* and in isolated atrial preparations, isolated SAN myocytes from AngII-infused mice had reductions in spontaneous AP firing frequency and DD slope in basal conditions as well as smaller increases in AP firing frequency and DD slope after application of ISO (10 nM; *Figure 2A–E*). ISO increased action potential duration at 50% repolarization (APD_{50}) in SAN myocytes from saline- and AngII-infused mice to a similar extent (see Supplementary material online, *Table S2*). There were no differences in maximum diastolic potential or any other measurements of SAN AP morphology between treatment groups in control conditions or in response to ISO (see Supplementary material online, *Table S2*).

I_f and $I_{Ca,L}$ are each importantly involved in mediating β-AR dependent increases in DD slope and HR.[6] Accordingly, the effects of ISO (10 nM) on I_f and $I_{Ca,L}$ were measured in isolated SAN myocytes from saline- and AngII-infused mice. I_f density was reduced in control conditions and after application of ISO in AngII-infused mice (*Figure 2F–H*). While ISO increased I_f density in both groups, the increase in I_f density was smaller in SAN myocytes from AngII-infused mice (*Figure 2H*, Supplementary material online, *Figure S4*). Analysis of I_f steady-state activation kinetics shows that the voltage for 50% channel activation ($V_{1/2(act)}$) was not different between groups in control conditions; however, ISO induced a smaller shift in $V_{1/2(act)}$ in SAN myocytes from AngII-infused mice compared to saline-infused controls (*Figure 2I* and *J*, Supplementary material online, *Figure S4*, Supplementary material online, *Table S3*). No differences were observed in the slope factor for I_f activation at baseline or in response to ISO (see Supplementary material online, *Table S3*).

There were no differences in SAN $I_{Ca,L}$ density at baseline between saline- and AngII-infused mice (*Figure 2K* and *L*). ISO (10 nM) increased $I_{Ca,L}$ density in both groups; however, the magnitude of the increase was smaller in SAN myocytes from AngII-infused mice (*Figure 2M*, Supplementary material online, *Figure S5*). Analysis of $I_{Ca,L}$ steady-state activation kinetics showed that maximum conductance (G_{max}), $V_{1/2(act)}$, and $I_{Ca,L}$ slope factor were not different at baseline between saline- and AngII-infused mice (*Figure 2N*, Supplementary material online, *Figure S5*, Supplementary material online, *Table S4*). In response to ISO, AngII-infused mice had smaller increases in $I_{Ca,L}$, G_{max}, and $V_{1/2(act)}$ compared to saline-infused controls (*Figure 2N* and *O*, Supplementary material online, *Table S4*). There were no differences in the slope factor for $I_{Ca,L}$ activation between saline- and AngII-infused mice after application of ISO (see Supplementary material online, *Table S4*).

Consistent with AP data, CaT frequency was lower in SAN myocytes from AngII-infused mice in control conditions (see Supplementary material online, *Figure S6*). Application of ISO increased CaT frequency in SAN myocytes from saline- and AngII-infused mice, but the increase was smaller in AngII SAN myocytes (see Supplementary material online, *Figure S6*). There were no differences in SAN myocyte CaT amplitude or decay times in control conditions between saline- and AngII-infused mice (see Supplementary material online, *Figure S6*). ISO (10 nM) increased CaT amplitude (see Supplementary material online, *Figure S6A–C*) and shortened CaT decay times; however, these responses to ISO were reduced in AngII SAN myocytes compared to saline controls (see Supplementary material online, *Figure S6*).

3.4 PDE4D desensitizes β-ARs in the SAN in AngII-infused mice

Impaired β-AR signalling could occur due to down-regulation of β-ARs in SAN myocytes or disruption of downstream cAMP signalling.[13,31] There were no differences in protein levels of β_1- and β_2-ARs in the SAN between saline- and AngII-infused hearts (see Supplementary material online, *Figure S7A and B*). Despite this, ISO (10 nM) induced smaller increases in intracellular cAMP in SAN myocytes from AngII-infused mice (*Figure 3A*). PDE4D is a major regulator of cAMP production following β-AR activation in murine hearts.[32] Whole cell SAN PDE4D levels were not different between groups (*Figure 3B* and *C*); however, phosphorylated PDE4D was elevated in the SAN of AngII-infused mice (*Figure 3D*). Consistent with this, there was an increase in whole cell PDE4 activity in the SAN of AngII-infused mice (*Figure 3E*).

Immunocytochemistry was used to determine the co-localization of PDE4D with β-ARs in SAN myocytes from saline- and AngII-infused mice (*Figure 3F* and *G*). These data demonstrate that the co-localization of PDE4D with β_1- and β_2-ARs was increased in AngII SAN myocytes (*Figure 3H* and *I*). Co-immunoprecipitation of β_1- and β_2-ARs with PDE4D also demonstrated increased PDE4D localization surrounding both β-ARs in the SAN of AngII-infused mice (*Figure 3J* and *K*). There were no differences in the mRNA expression of any of the major cardiac PDE4 isoforms in the SAN after AngII infusion (see Supplementary material online, *Figure S7C*).

3.5 PDE4D knockdown increases SAN β-AR responsiveness in AngII-infused hearts

To investigate the role of PDE4D in regulating β-AR signalling in the SAN, mice were injected retro-orbitally with an AAV9 carrying an shRNA for the murine PDE4D isoform (or scrambled control) (*Figure 4A*). Five weeks after AAV9 injection at 1.5×10^{11} genomic copies/mouse, robust infection of the right atrial posterior wall was observed (see Supplementary material online, *Figure S8*), which resulted in a ~65% knockdown of PDE4D in SAN tissue (*Figure 4B* and *C*).

First, the effects of PDE4D knockdown (PDE4D KD) were investigated in normal mice. There were no differences in HR in anaesthetized mice in

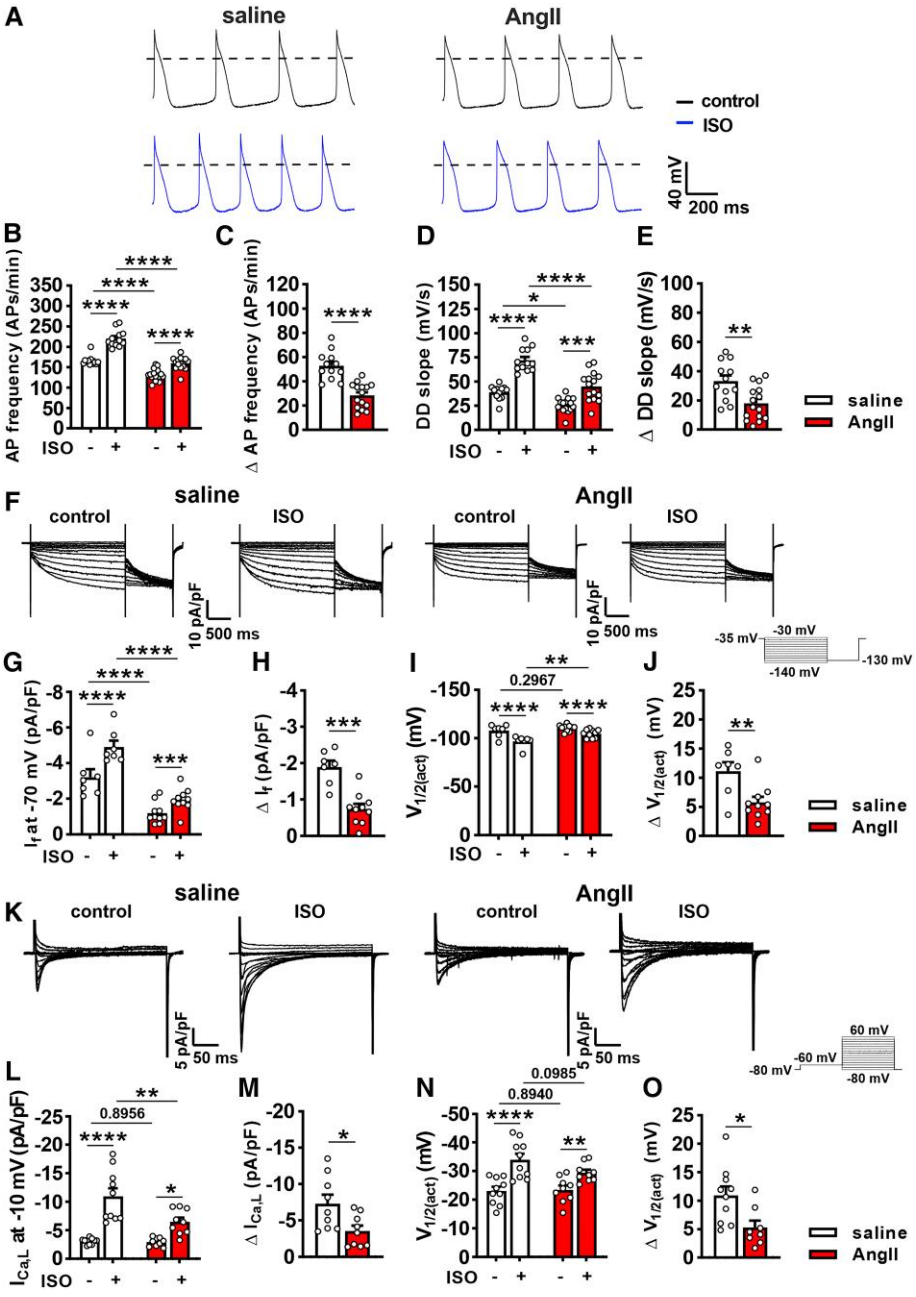

Figure 2 Effects of β-AR stimulation on SAN myocyte electrophysiology in AngII-infused mice. (*A*) Representative spontaneous APs in isolated SAN myocytes from saline- and AngII-infused mice in control conditions and after superfusion of ISO (10 nM). Scale bars apply to all recordings. (*B* and *C*) Summary of AP firing frequency in control conditions and after application of ISO (*B*) and the change in AP firing frequency after ISO (*C*). (*D* and *E*) Summary of SAN myocyte DD slope in control conditions and after application of ISO (*D*) and the change in DD slope after application of ISO (*E*). $n = 12$ cells from four mice for saline and 15 cells from five mice for AngII. See Supplementary material online, *Table S2* for additional AP morphology parameters. (*F*) Representative I_f recordings in isolated SAN myocytes from saline- and AngII-infused mice in control conditions and after superfusion of ISO (10 nM). Voltage clamp protocol shown to the right of the recordings. (*G* and *H*) I_f density at −70 mV in control conditions and after application of ISO (*G*) and the change in I_f density after application of ISO (*H*). (*I* and *J*) I_f $V_{1/2(act)}$ in control conditions and after application of ISO (*I*) and the change in I_f $V_{1/2(act)}$ after application of ISO (*J*). $n = 7$ cells from four mice for saline and 10 cells from seven mice for AngII. Full I_f IV curves and steady-state activation curves are provided in Supplementary material online, *Figure S4*. Refer to Supplementary material online, *Table S3* for additional I_f analysis. (*K*) Representative $I_{Ca,L}$ recordings in isolated SAN myocytes from saline- and AngII-infused mice in control conditions and after superfusion of ISO (10 nM). Voltage clamp protocol shown to the right of the recordings. (*L* and *M*) $I_{Ca,L}$ density at −10 mV in control conditions and after application of ISO (*L*) and the change in $I_{Ca,L}$ density after application of ISO (*M*). (*N* and *O*) $I_{Ca,L}$ $V_{1/2(act)}$ in control conditions and after application of ISO (*N*) and the change in $I_{Ca,L}$ $V_{1/2(act)}$ after application of ISO (*O*). $n = 9$ cells from four mice for saline and 8 cells from five mice for AngII. Full $I_{Ca,L}$ IV curves and steady-state activation curves are provided in Supplementary material online, *Figure S5*. Refer to Supplementary material online, *Table S4* for additional $I_{Ca,L}$ analysis. Panels *B*, *D*, *G*, *I*, *L*, and *N* analysed by two-way repeated measures ANOVA with Holm-Sidak *post hoc* test. Panels *C*, *E*, *H*, *J*, *M*, and *O* analysed by Student's *t*-test.

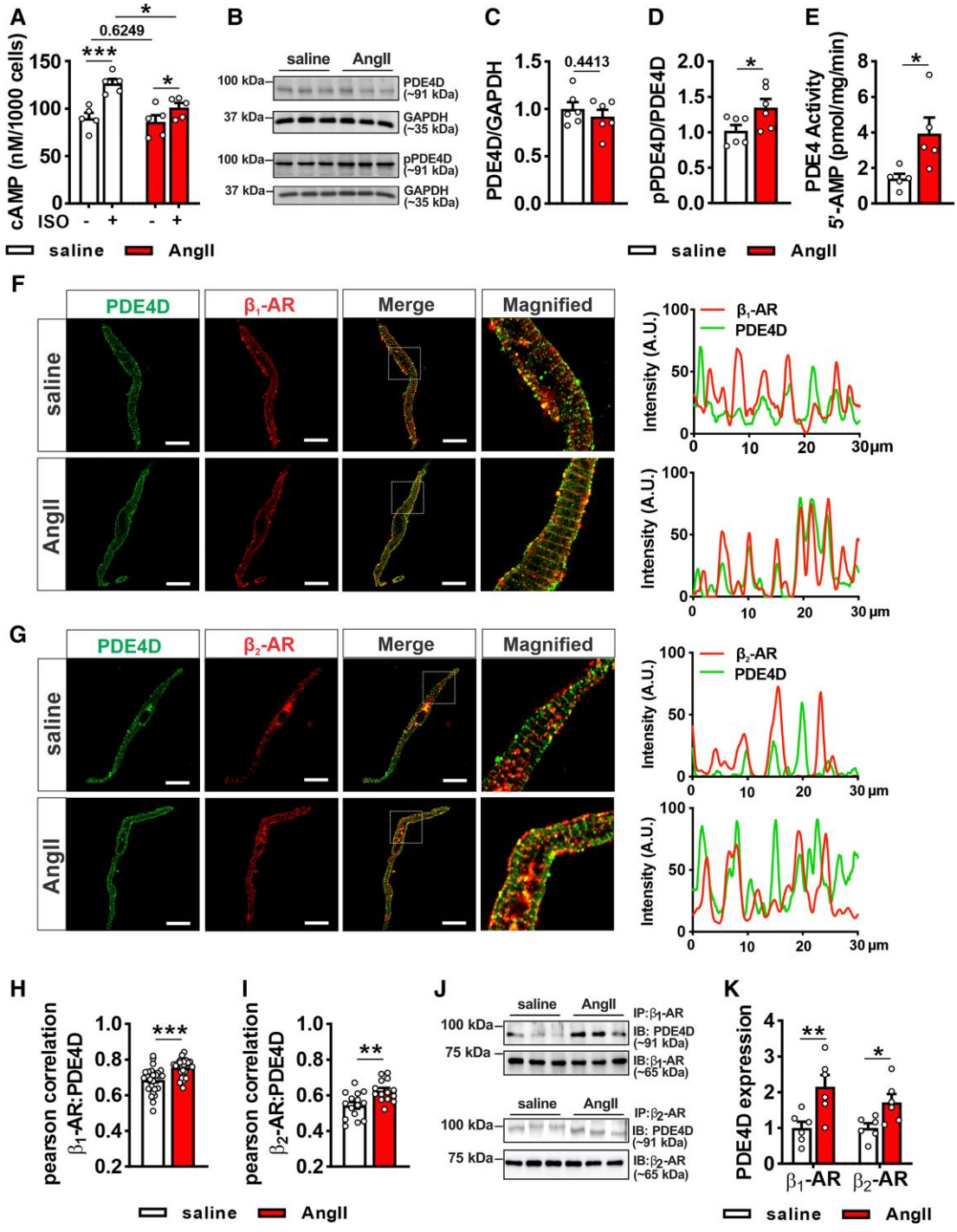

Figure 3 Increased PDE4D activity and localization with β-ARs in the SAN in AngII-infused mice. (*A*) Summary of cAMP levels before and after application of ISO (10 nM) in SAN myocytes from saline ($n = 5$ pooled SAN) and AngII ($n = 5$ pooled SAN) infused mice. Data analysed by two-way ANOVA with Holm-Sidak *post hoc* test. (*B–D*) Representative whole cell lysate western blots (*B*) and summary of protein expression of PDE4D (*C*) and phosphorylated PDE4D (*D*) in the SAN in saline ($n = 6$ pooled SAN) and AngII-infused ($n = 6$ pooled SAN) mice. Data analysed by Student's *t*-test. (*E*) Whole cell lysate PDE4 activity in the SAN of saline ($n = 5$ pooled SAN) and AngII-infused ($n = 5$ pooled SAN) mice. Data analysed by Student's *t*-test. (*F* and *G*) Immunocytochemistry showing fluorescent images of PDE4D, β_1-AR (*F*), and β_2-AR (*G*) and merged images in SAN myocytes from saline- and AngII-infused mice. Boxes in the merged images are shown in the magnified views. Representative intensity plots illustrate overlap of PDE4D with β_1-ARs and β_2-ARs in SAN myocytes from saline- and AngII-infused mice. (*H* and *I*) Pearson correlations of overlap of PDE4D with β_1-ARs (*H*; $n = 26$ myocytes from three saline mice and 25 myocytes from three AngII mice) and β_2-ARs (*I*; $n = 15$ myocytes from three saline mice and 14 myocytes from three AngII mice). Data analysed by Student's *t*-test. (*J* and *K*) Representative β_1- and β_2-AR co-immunoprecipitation western blots (*F*) and summary of PDE4D expression surrounding β_1- and β_2-ARs in the SAN of saline ($n = 6$ pooled SAN) and AngII-infused ($n = 6$ pooled SAN) mice (*G*). Data analysed by two-way ANOVA with Holm-Sidak *post hoc* test. Uncropped western blots are provided in Supplementary material online, *Figure S15*.

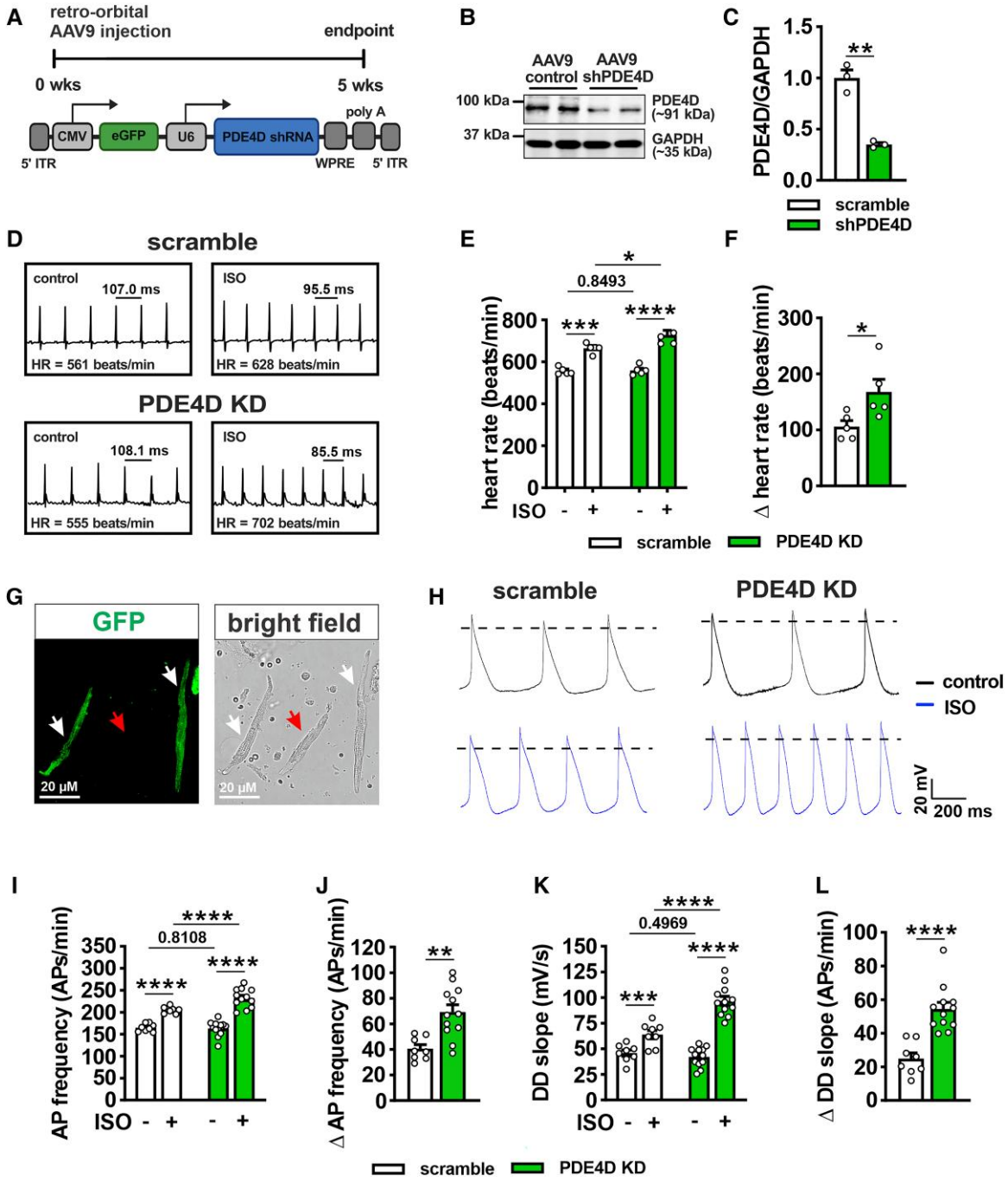

Figure 4 PDE4D knockdown regulates β-AR signalling in the SAN. (*A*) Schematic of AAV9 PDE4D shRNA. (*B* and *C*) PDE4D protein levels in the SAN 5 weeks after injection of mice with a scrambled shRNA (AAV9-control; $n = 3$) and the PDE4D shRNA (AAV9-shPDE4D; $n = 3$). Data analysed by Student's *t*-test. Uncropped western blots are provided in Supplementary material online, *Figure S15*. (*D*) Representative ECGs in anaesthetized PDE4D knockdown (PDE4D KD) mice and scramble controls in control conditions and following acute intraperitoneal injection of ISO (10 mg/kg). (*E* and *F*) Summary of HR in control conditions and after injection of ISO (*E*) and change in HR in response to ISO (*F*) in PDE4D KD mice ($n = 5$) and scramble controls ($n = 5$). Data in panel *E* analysed by two-way ANOVA with Holm-Sidak *post hoc* test. Data in panel *F* analysed by Student's *t*-test. (*G*) Representative image showing AAV9 infected SAN myocytes (GFP^+; white arrows) and non-infected myocytes (red arrow). Only GFP^+ myocytes were used in patch-clamp experiments. (*H*) Spontaneous APs in isolated SAN myocytes from PDE4D KD and scramble control mice in control conditions and after superfusion of ISO (10 nM). Scale bars apply to all recordings. (*I* and *J*) AP firing frequency in control conditions and after application of ISO (*I*) and change in AP firing frequency after application of ISO (*J*). (*K* and *L*) DD slope in control conditions and after application of ISO (*K*) and change in DD slope after application of ISO (*L*). Refer to Supplementary material online, *Table S5* for additional AP analysis. $n = 8$ myocytes from three mice from scramble and 12 myocytes from three mice for PDE4D KD. Data in panels *I* and *K* analysed by two-way repeated measures ANOVA with Holm-Sidak *post hoc* test. Data in panels *J* and *L* analysed by Student's *t*-test.

control conditions between PDE4D KD and scrambled controls; however, acute application of ISO (10 mg/kg) resulted in larger increases in HR in PDE4D KD mice compared to a scrambled shRNA (*Figure 4D–F*). Next, SAN myocytes were isolated from PDE4D KD and scramble control mice, and GFP positive cells were used to assess SAN AP morphology and β-AR sensitivity (*Figure 4G*). Spontaneous AP recordings in these GFP^+ SAN myocytes demonstrate that AP frequency was comparable in control conditions; however, ISO induced larger increases in AP firing frequency after PDE4D KD (*Figures 4I* and *J*). Similarly, DD slope was comparable in control conditions, but increased to a greater extent after ISO application in PDE4D KD myocytes (*Figure 4K* and *L*). Additional AP parameters are provided in Supplementary material online, *Table S5*.

Next, the role of PDE4D in the SAN was investigated in PDE4D knockdown mice infused with AngII. The effects of an acute injection of ISO (10 mg/kg) on HR were measured in saline, AngII-scramble, and AngII-PDE4D knockdown (AngII-PDE4D KD) mice. As expected, AngII-scramble mice had smaller increases in HR following ISO injection (*Figure 5A–C*). In contrast, AngII-PDE4D KD mice showed substantially improved ISO-induced increases in HR that were similar to saline controls (*Figure 5B* and *C*).

Hearts from the same mice used for these *in vivo* experiments were subsequently isolated and used for optical mapping studies. Activation maps and OAPs from the SAN region of the right atrial posterior wall (*Figure 5D*) were used to assess SAN electrical activation and conduction in response to β-AR stimulation. Consistent with the improvements in β-AR signalling observed *in vivo*, isolated atrial preparations from AngII-PDE4D KD mice had improved beating rate responses to ISO compared to AngII-scramble controls (*Figure 5E* and *F*). Furthermore, AngII-PDE4D-KD mice had improved effects of ISO on CV (*Figure 5G* and *H*) as well as larger increases in DD slope compared to AngII-scramble mice (*Figure 5I* and *J*). While SAN chronotropic responses to β-AR stimulation were largely normalized in atrial preparations from AngII-PDE4D-KD mice, initial activation sites in the SAN still exhibited substantial heterogeneity in control conditions compared to saline hearts. Nevertheless, the majority of activation sites still shifted superiorly in response to ISO in PDE4D KD mice (see Supplementary material online, *Figure S9*).

3.6 PDE4D knockdown enhances β-AR signalling in SAN myocytes from AngII-infused mice

The effects of PDE4D knockdown on β-AR responsiveness in isolated GFP^+ SAN myocytes were also measured (*Figure 6*). SAN myocytes from AngII-PDE4D KD mice exhibited increased AP firing frequency and DD slope responses to ISO (10 nM) that were larger than those observed in AngII-scramble SAN myocytes and comparable to SAN myocytes from saline mice (*Figure 6A–E*, Supplementary material online, *Table S6*). While the magnitude of the responses to ISO were normalized, peak AP firing frequency and DD slope were still lower in AngII-PDE4D-KD mice compared to SAN myocytes from saline mice (see Supplementary material online, *Table S6*), likely due to the presence of intrinsic SAN dysfunction due to HCN4 down-regulation.[24] There were no differences in other measurements of SAN AP morphology between treatment groups in control conditions or in response to ISO (see Supplementary material online, *Table S6*).

I_f density was still reduced in AngII-PDE4D KD SAN myocytes to similar levels as AngII-scramble SAN myocytes in control conditions; however, SAN myocytes from AngII-PDE4D KD mice had larger increases in I_f density following ISO (10 nM) application that were similar in magnitude to saline controls (*Figure 7A–C*, Supplementary material online, *Figure S10*). Analysis of I_f activation kinetics showed that ISO induced comparable shifts in $V_{1/2(act)}$ in saline- and AngII-PDE4D KD SAN myocytes (*Figure 7D* and *E*, Supplementary material online, *Figure S10*, Supplementary material online, *Table S7*). No differences in the slope factor for I_f activation were seen at baseline or in response to ISO between any groups (see Supplementary material online, *Table S7*).

SAN $I_{Ca,L}$ density showed no differences at baseline between saline, AngII-scramble, or AngII-PDE4D-KD SAN myocytes (*Figure 7F* and *G*). ISO (10 nM) increased $I_{Ca,L}$ density in all groups; however, SAN myocytes from AngII-scramble mice had smaller increases in $I_{Ca,L}$ density compared to saline mice while SAN myocytes from AngII-PDE4D KD mice had increases in $I_{Ca,L}$ density that were comparable to saline controls (*Figure 7G* and *H*, Supplementary material online, *Figure S11*). Analysis of $I_{Ca,L}$ activation kinetics showed that G_{max}, $V_{1/2(act)}$, and slope factor were not different at baseline between groups (*Figure 7I*, Supplementary material online, *Figure S11*, Supplementary material online, *Table S8*). In response to ISO, AngII-PDE4D KD SAN myocytes had larger increases in $I_{Ca,L}$ G_{max} and $V_{1/2(act)}$ compared to AngII-scramble SAN myocytes, which were indistinguishable from saline-infused mice (*Figure 7I* and *J*, Supplementary material online, *Figure S11*, Supplementary material online, *Table S8*).

ISO (10 nM) also increased CaT frequency, increased CaT amplitude, and reduced CaT decay times in SAN myocytes from saline, AngII-scramble and AngII-PDE4D KD (see Supplementary material online, *Figure S12*). These effects of ISO were impaired in SAN myocytes isolated from AngII-scramble mice compared to saline SAN mice, however, the effects of ISO on CaT morphology were normalized in AngII-PDE4D KD SAN myocytes (see Supplementary material online, *Figure S12*).

To confirm the results of PDE4D knockdown, the effects of the selective PDE4 inhibitor rolipram[11] (Rol; 10 μM) on β-AR responsiveness were measured in isolated SAN myocytes from saline- and AngII-infused mice (see Supplementary material online, *Figure S13*). As expected, ISO increased AP firing frequency in both groups with smaller increases observed in SAN myocytes from AngII-infused mice (see Supplementary material online, *Figure S13A–C*). Addition of Rol in the presence of ISO further increased AP firing frequency in both groups; however, these effects were larger in SAN myocytes from AngII-infused mice (see Supplementary material online, *Figure S13C and D*). Similarly, Rol enhanced ISO-induced increases in DD slope in both saline- and AngII-infused mice (see Supplementary material online, *Figure S13E–G*) and normalized the increase in DD slope in SAN myocytes from AngII-infused mice (see Supplementary material online, *Figure S13F and G*). Consistent with these improvements in AP firing frequency and DD slope, Rol also produced larger increases in I_f (see Supplementary material online, *Figure S13H–J*) and $I_{Ca,L}$ (see Supplementary material online, *Figure S13K–M*) in ISO-stimulated SAN myocytes from AngII-infused mice compared to saline controls.

PDE3A is also an important regulator of SAN function; therefore, the effects of the selective PDE3 inhibitor milrinone (Mil; 10 μM) on AP morphology were measured in SAN myocytes from saline- and AngII-infused mice (see Supplementary material online, *Figure S14*). Sequential application of ISO (10 nM), and then Mil in the presence of ISO, caused similar increases in AP firing frequency and DD slope in SAN myocytes from saline- and AngII-infused mice (see Supplementary material online, *Figure S14A–E*). AP firing frequency and DD slope remained reduced in AngII-infused SAN myocytes after application of ISO and Mil. Consistent with this, there were no differences in *pde3a* mRNA expression or PDE3A protein levels in the SAN between saline- and AngII-infused mice (see Supplementary material online, *Figure S14F–H*).

4. Discussion

Appropriate HR regulation by the sympathetic nervous system is critical for proper maintenance of cardiac function. In diseases such as hypertensive heart disease and heart failure, HR regulation becomes impaired due to progressive SAN dysfunction and β-AR desensitization.[7,21] Nevertheless, the mechanisms for impaired β-AR regulation of HR in these settings have been poorly understood. In the present study, we used a multi-level approach to assess β-AR regulation of HR and SAN function in mice with AngII-induced hypertensive heart disease. Our findings demonstrate that impaired HR regulation by β-AR activation in AngII-infused mice is due to increased PDE4 activity and PDE4D co-localization with β-ARs in the

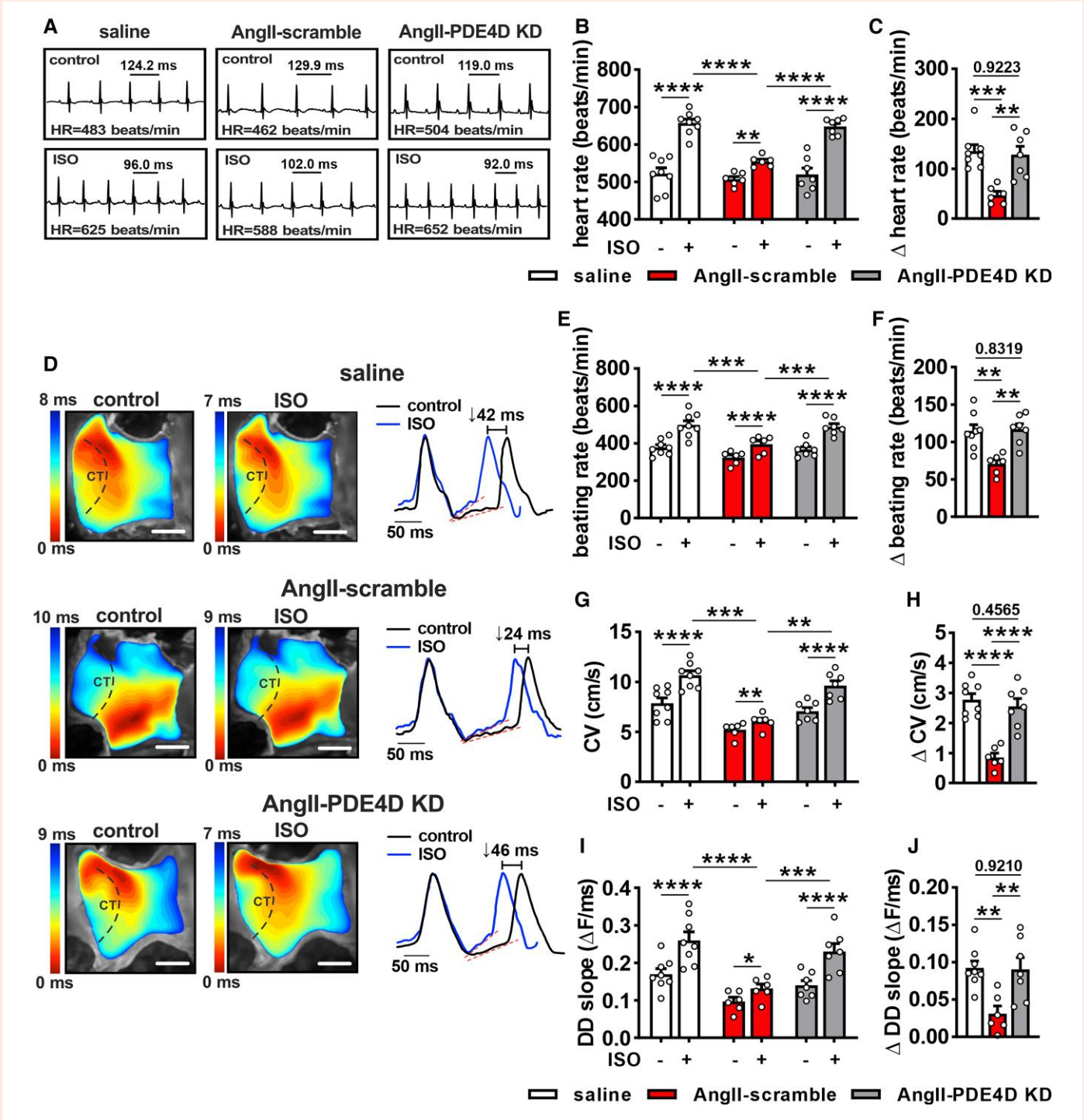

Figure 5 PDE4D knockdown normalizes β-AR responsiveness in AngII-infused mice. (*A–C*) Representative ECGs (*A*), summary of heart rate in control conditions and after intraperitoneal injection of ISO (10 mg/kg; *B*), and change in heart rate after injection of ISO (*C*) for saline ($n = 8$), AngII-scramble ($n = 6$), and AngII-PDE4D KD ($n = 7$) mice. (*D*) Representative activation maps and OAPs in isolated atrial preparations from saline, AngII-scramble, and AngII-PDE4D KD mice in control conditions and after superfusion of ISO (10 nM). Dashed lines indicate the crista terminalis (CT). Scale bar = 2 mm. Red lines on OAPs represent linear fitting of diastolic depolarization (DD) slope. (*E–J*) Summary data in control conditions and after application of ISO as well as Δ values after ISO application for heart rate (*E* and *F*), CV in the SAN region of the right atrial posterior wall (*G* and *H*), and OAP DD slope (*I* and *J*) for saline ($n = 8$), AngII-scramble ($n = 6$), and AngII-PDE4D KD ($n = 7$) mice. Data in panels *B*, *E*, *G*, and *I* analysed by two-way repeated measures ANOVA with Holm-Sidak *post hoc* test. Data in panels *C*, *F*, *H*, and *J* analysed by one-way ANOVA with Holm-Sidak *post hoc* test.

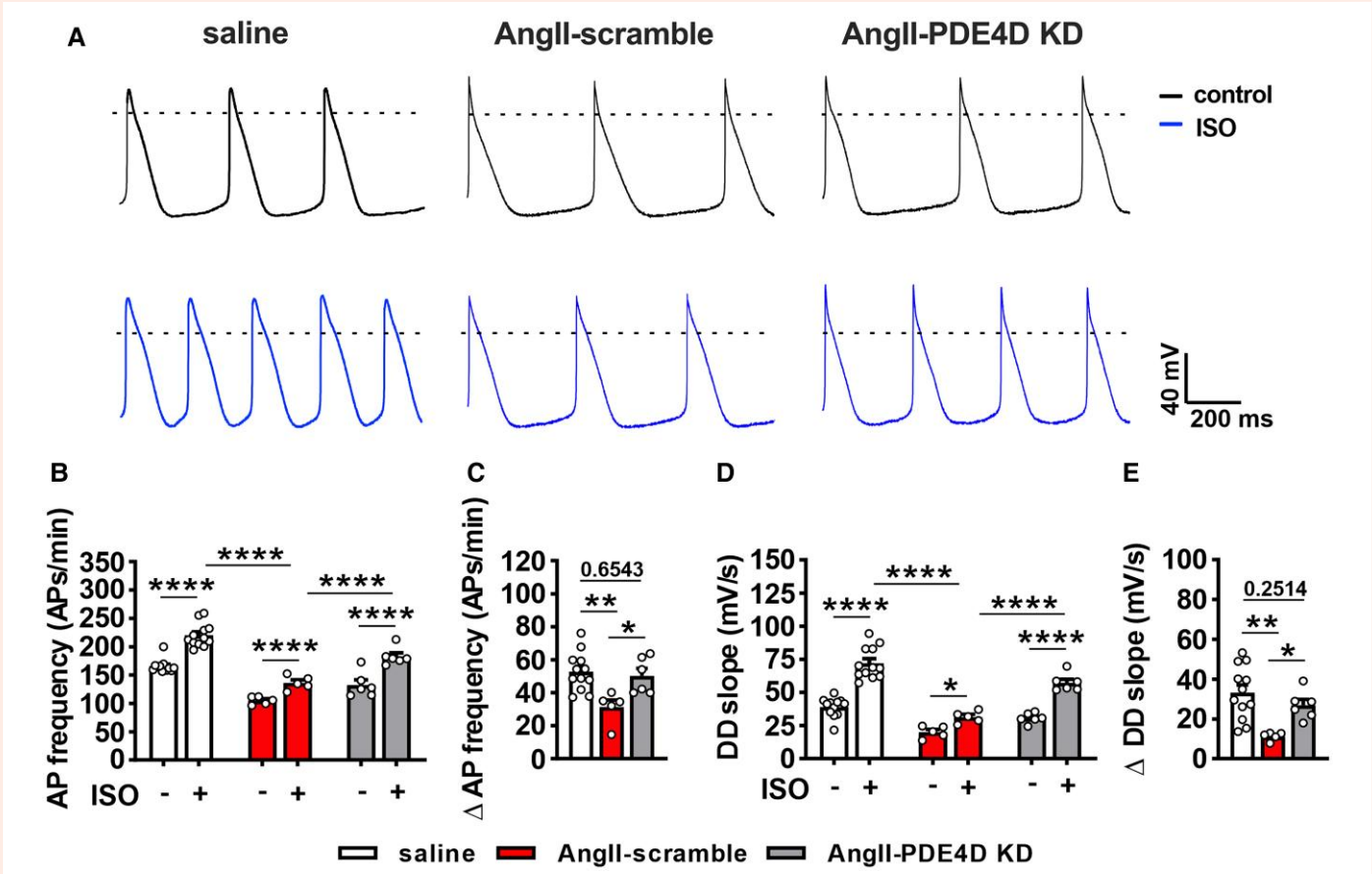

Figure 6 PDE4D knockdown normalizes the effects of isoproterenol on spontaneous AP firing in isolated SAN myocytes from AngII-infused mice. (*A*) Representative spontaneous APs in isolated SAN myocytes from saline, AngII-scramble, and AngII-PDE4D KD mice in control conditions and after superfusion of ISO (10 nM). Scale bars apply to all recordings. (*B* and *C*) AP firing frequency in control conditions and after application of ISO (*B*) and change in AP firing frequency after application of ISO (*C*). (*D* and *E*) DD slope in control conditions and after application of ISO (*D*) and change in DD slope after application of ISO (*E*). Refer to Supplementary material online, *Table S6* for additional AP analysis. $n = 12$ cells from four mice for saline, 5 cells from three mice for AngII-scramble, and 6 cells from three mice for AngII-PDE4D KD. Data in panels *C* and *E* analysed by two-way ANOVA with Holm-Sidak *post hoc* test. Data in panels *D* and *F* analysed by one-way ANOVA with Holm-Sidak *post hoc* test.

SAN, which altered cAMP-dependent regulation of spontaneous AP firing in SAN myocytes. AP firing was impaired due to reduced effects of β-AR agonists on I_f and $I_{Ca,L}$ in SAN myocytes. These findings provide new insight into the mechanisms of chronotropic incompetence in the setting of hypertensive heart disease.

AngII infusion is a well characterized and clinically relevant model of heart disease.[33,34] Hypertension is the number one risk factor for the development of heart failure,[2,35] and these individuals exhibit high levels of circulating plasma AngII.[36] Our present study, as well as our prior work,[24,27,28] shows that AngII-infused mice develop overt cardiac hypertrophy without reductions in ejection fraction or fractional shortening. AngII infusion also caused increases in right and left atrial area, which is an indication of diastolic dysfunction.[37] In conscious mice, AngII infusion resulted in elevated HR during low activity, but lower HR during high activity as well as lower intrinsic HR (i.e. during autonomic blockade), indicating impaired SAN function and increased sympathetic nervous system activity that collectively result in an inability to increase HR in response to increasing activity levels. This is consistent with previous studies demonstrating elevated circulating norepinephrine levels in AngII-infused mice.[23]

Consistent with a chronotropic incompetence phenotype, injection of the β-AR agonist ISO resulted in smaller HR increases in AngII-infused mice. Similar findings in human heart failure with preserved ejection fraction patients show that graded ISO infusions produced smaller increases in HR compared to age-matched controls[21] further supporting the hypothesis that impaired HR regulation is due to impaired β-AR signalling in the SAN. While our model of AngII infusion for three weeks does not induce heart failure with marked systolic dysfunction, our findings suggest that chronotropic incompetence manifests early in the progression from hypertensive heart disease to overt heart failure. Consistent with this, hypertension patients display a higher frequency of chronotropic incompetence compared to normotensive controls.[38] Furthermore, chronotropic incompetence is a powerful predictor of the presence of heart failure symptoms in patients with hypertension.[9]

SAN dysfunction was evident in AngII-infused mice in baseline (control) conditions as indicated by a progressive decline in intrinsic beating rate *in vivo* and in isolated atrial preparations. We have previously demonstrated that intrinsic SAN dysfunction, as well as impairments in conduction and variability in leading activation site, occur in control conditions in AngII mice due to impaired SAN AP firing and fibrosis in the SAN.[23,24] In the present study, we found that in conjunction with intrinsic SAN dysfunction, atrial preparations from AngII-infused mice exhibited smaller increases in beating rate, CV, and DD slope during spontaneous AP firing in response to ISO compared to saline controls. In healthy hearts, β-AR stimulation shifts the leading activation site to a more superior location in the

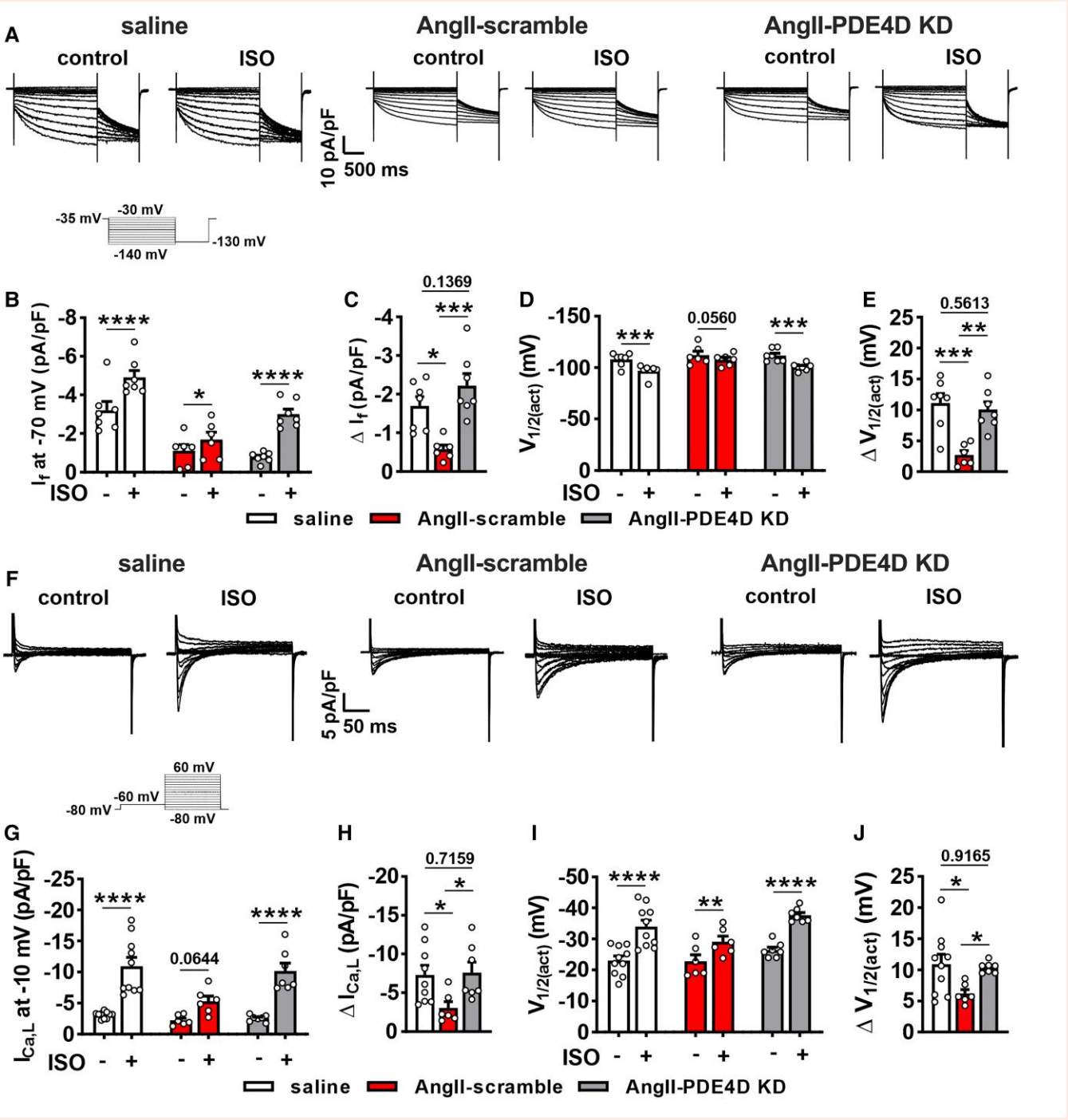

Figure 7 PDE4D knockdown normalizes the effects of ISO on I_f and $I_{Ca,L}$ in isolated SAN myocytes from AngII-infused mice. (*A*) Representative I_f recordings in isolated SAN myocytes from saline, AngII-scramble, and AngII-PDE4D KD mice in control conditions and after superfusion of ISO (10 nM). Scale bars apply to all recordings. Voltage clamp protocol shown below recordings. (*B* and *C*) I_f density at −70 mV in control conditions and after application of ISO (*B*) and change in I_f density after ISO (*C*) in saline, AngII-scramble, and AngII-PDE4D KD SAN myocytes. (*D* and *E*) I_f $V_{1/2(act)}$ in control conditions and after application of ISO (*D*) and change in I_f $V_{1/2(act)}$ after ISO (*E*) in saline, AngII-scramble, and AngII-PDE4D KD SAN myocytes. $n = 7$ cells from four mice for saline, 6 cells from three mice for AngII-scramble, and 7 cells from three mice for AngII-PDE4D KD. Full I_f IV curves and I_f steady-state activation curves are provided in Supplementary material online, *Figure S10*. Refer to Supplementary material online, *Table S7* for additional I_f analysis. (*F*) Representative $I_{Ca,L}$ recordings in isolated SAN myocytes from saline, AngII-scramble, and AngII-PDE4D KD mice in control conditions and after superfusion of ISO (10 nM). Scale bars apply to all recordings. Voltage clamp protocol shown below recordings. (*G–J*) $I_{Ca,L}$ density at −10 mV in control conditions and after application of ISO (*G*) and change in $I_{Ca,L}$ density after ISO (*H*) in saline, AngII-scramble, and AngII-PDE4D KD SAN myocytes. (*I* and *J*) $I_{Ca,L}$ $V_{1/2(act)}$ in control conditions and after application of ISO (*I*) and change in $I_{Ca,L}$ $V_{1/2(act)}$ after ISO (*J*) in saline, AngII-scramble, and AngII-PDE4D KD SAN myocytes. $n = 9$ cells from four mice for saline, 6 cells from three mice for AngII-scramble, and 7 cells from three mice for AngII-PDE4D KD. Full $I_{Ca,L}$ IV curves and $I_{Ca,L}$ steady-state activation curves are provided in Supplementary material online, *Figure S11*. Refer to Supplementary material online, *Table S8* for additional $I_{Ca,L}$ analysis. Data in panels *B*, *D*, *G*, and *I* analysed by two-way repeated measures ANOVA with Holm-Sidak *post hoc* test. Data in panels *C*, *E*, *H*, and *J* analysed by one-way ANOVA with Holm-Sidak *post hoc* test.

SAN[29,30,39] as we observed in saline-infused mice. In contrast, AngII-infused mice had variable changes in initial activation sites following β-AR stimulation and exhibited arrhythmias such as sinus pauses and rapid ectopic activity resembling brady-tachy rhythms commonly seen in individuals with heart disease and SAN dysfunction.[40,41]

Impaired ISO-induced increases in AP firing frequency in isolated SAN myocytes from AngII-infused mice occurred in association with smaller ISO-induced increases I_f and $I_{Ca,L}$ as well as smaller ISO effects on CaT frequency and morphology. ISO increases I_f conductance via the binding of cAMP to HCN channels, negatively shifting the $V_{1/2(act)}$.[5,6,42] ISO also increases $I_{Ca,L}$ density and activation kinetics via cAMP and PKA in SAN myocytes.[6] These effects on I_f and $I_{Ca,L}$ both contribute importantly to the stimulatory effects of ISO on SAN AP frequency.[6,43] SAN myocytes from AngII-infused mice had smaller shifts in $V_{1/2(act)}$ for both I_f and $I_{Ca,L}$ in response to ISO compared to saline controls, which is consistent with reduced cAMP levels in the SAN after AngII infusion.

The impaired effects of ISO on SAN myocyte AP firing also occurred in association with reduced effects on CaT morphology. Local Ca^{2+} releases during the diastolic period, prior to the CaT, also contribute to the generation of the diastolic depolarization, and these processes are cAMP dependent. This creates a 'coupled clock' mechanism for spontaneous AP firing.[5,10] The observation of reduced effects of ISO on membrane currents as well as CaT morphology indicates that multiple cAMP-dependent components that are downstream of the β-ARs, including ion channels and Ca^{2+} regulatory proteins, contribute to chronotropic incompetence in AngII-mediated heart disease.

These findings are consistent with previous studies showing that cAMP generation, assessed by high-resolution FRET-based imaging in SAN myocytes from mice with heart failure, is reduced following β-AR stimulation.[44] Moreover, a recent study in a rat model of heart failure with preserved ejection fraction also demonstrated chronotropic incompetence due to altered SAN electrophysiological responses to β-AR stimulation, although the mechanisms leading to impaired β-AR signalling were not identified in that study.[20] Similar to other studies of SAN dysfunction in heart disease models,[20] we did not observe changes in β-AR expression in the SAN. Conversely, changes in β-AR expression have been well documented in the ventricular myocardium of patients with hypertensive heart disease.[31,45] This indicates that regulation of β-AR expression in the SAN in hypertensive heart disease and heart failure is distinct from the working myocardium.

PDEs are a family of enzymes that critically regulate cyclic nucleotide signalling by compartmentalizing cAMP (and cGMP) signalling cascades.[13,32] PDE4 isoforms are primarily responsible for the degradation of cAMP at high intracellular concentrations such as following β-AR stimulation.[46] Total PDE4 activity, measured using rolipram, was found to be increased in the SAN in AngII-infused mice. Subsequent studies demonstrated increased levels of phosphorylated PDE4D and increased PDE4D co-localization with β_1- and β_2-ARs in the SAN of AngII-infused mice. Enhanced PDE4D recruitment to β-ARs is well defined[16,17,47–49] and can be initiated by multiple neurohumoral factors such as high levels of catecholamine stimulation[49] or even directly by AngII.[16] While this can provide a negative feedback mechanism whereby phosphorylation of PDE4D by PKA or other kinases increases its hydrolytic activity for cAMP and facilitates recruitment to β-ARs to prevent excessive catecholamine signalling,[50] the present study demonstrates that changes in PDE4D activity and localization lead to impaired HR responses and SAN function in AngII-mediated heart disease.

To confirm the role of PDE4D in AngII-mediated β-AR desensitization, we utilized an AAV9-mediated PDE4D knockdown model that produced ~65% knockdown of PDE4D in the SAN. In normal mice, PDE4D KD did not have major effects on basal HR *in vivo* or on SAN AP firing frequency in control conditions. In contrast, ISO elicited much larger increases in HR and SAN AP firing frequency in PDE4D KD mice, which is consistent with a role for PDE4D in regulating cAMP during β-AR stimulation in the SAN.

Critically, PDE4D knockdown largely normalized the magnitude of the effects of ISO on HR, CV, and DD slope in AngII-infused mice to levels that were comparable to saline controls. At a cellular level, this was due to the normalization of the effects of ISO on I_f, $I_{Ca,L}$, and CaT morphology in SAN myocytes. This is consistent with a previous study demonstrating that PDE4D knockout mice have exaggerated atrial cAMP responses to β-AR stimulation.[51] These findings demonstrate that the changes in PDE4D activity and localization identified here can account for the impaired responses to ISO in the SAN in AngII-mediated heart disease. Furthermore, these studies demonstrate that a partial reduction of PDE4D protein levels is sufficient to normalize PDE4D signalling in AngII-mediated hypertensive heart disease.

Our prior studies show that I_f is reduced and that $I_{Ca,L}$ is not different in control conditions (i.e. without ISO) in SAN myocytes from AngII-infused mice.[24] The basal reduction in I_f occurs in association with reduced HCN4 expression rather than a change in I_f steady-state activation kinetics.[24] Our present study is consistent with these prior results and explains why there are no differences in I_f or $I_{Ca,L}$ $V_{1/2(act)}$ in control conditions, including after PDE4D knockdown. This further supports the conclusion that PDE4D primarily controls cAMP during acute β-AR stimulation. We have also previously shown that the leading activation site in the right atrial posterior wall is more variable in AngII-infused mice, which was also seen in the present study. ISO is known to shift the leading activation site towards the superior region of the SAN,[30] which was observed in saline-infused mice in the present study, but less so in AngII-infused mice. Interestingly, after PDE4D knockdown, ISO induced superior shifts in leading activation site in most AngII-infused hearts, although the location of these leading activation sites remained more variable than in saline-infused hearts. The persistent variability, even after PDE4D knockdown, may be because of reductions in HCN4 expression and the presence of fibrosis in the SAN in AngII-infused mice.[24]

Acute application of rolipram, a specific PDE4 family inhibitor, increased SAN responsiveness to β-AR signalling by increasing ISO-stimulated spontaneous AP firing in SAN myocytes from AngII-infused mice. Interestingly, PDE4 inhibitors can augment catecholamine stimulated cAMP levels in human atria[51] but appear to have little inotropic effects in ventricular myocardium.[52] This may be due to differential expression and/or localization of PDE4 isoforms in atrial vs. ventricular myocardium. We have previously shown that in murine hearts, expression of PDE4D is ~two-fold higher in the SAN compared to the ventricles[11] consistent with a prominent role in regulating β-AR signalling in the SAN. Importantly, inhibition of PDE3 with milrinone did not improve ISO-responsiveness in SAN myocytes from AngII-infused mice, further supporting a primary role for PDE4 in chronotropic incompetence.

Some limitations of our study should be noted. In addition to the alterations identified in the present study, other factors may also contribute to chronotropic incompetence. For example, it is possible that compartmentalization of adenylyl cyclases or ion channels or changes in ion channel trafficking may occur. These could be investigated in future studies. While our studies demonstrate changes in SAN CaT morphology after ISO application in AngII-infused mice, a detailed analysis of sarcoplasmic reticulum Ca^{2+} handling and local Ca^{2+} release events during diastolic depolarization was not performed. The present study was conducted in a well-established model of hypertensive heart disease with cardiac hypertrophy. Future studies should investigate the role of PDE4D in the SAN in models of heart failure with preserved or reduced ejection fraction. Future studies could also investigate the impacts of PDE4D overexpression on β-AR function in the SAN in healthy and diseased hearts. From a translational perspective, it is important to recognize that the expression and regulation of PDE isoforms may differ between mice and humans. PDE4D regulation of β-AR function is well conserved between species[53]; however, it will be important to investigate the role of PDE4D in the SAN in human patients with hypertensive heart disease and heart failure in future studies.

5. Conclusion

AngII-induced hypertensive heart disease results in impaired HR responses to β-AR signalling due to up-regulation of PDE4D activity, particularly

around β-ARs in the SAN. Our findings identify new mechanisms for chronotropic incompetence and demonstrate a critical role for PDE4D in regulating SAN β-AR signalling. This may have important implications for understanding and treating SAN dysfunction in the setting of hypertensive heart disease.

Supplementary material

Supplementary material is available at *Cardiovascular Research* online.

Authors' contributions

T.W.D. and R.A.R. contributed to conception and experimental design. T.W.D. performed and analysed all experiments except immunocytochemistry that was performed by M.D.M. and echocardiography that was performed by D.D.B. T.W.D. and R.A.R. prepared the figures and wrote the manuscript. All authors read and approved the final manuscript.

Acknowledgements

The authors thank Dr Hailey Jansen for her assistance with some experiments.

Conflict of interest: None declared.

Funding

This work was supported by the Canadian Institutes of Health Research to R.A.R. (PJT166105 and PJT180474). T.W.D. held a Canadian Institutes of Health Research Doctoral Research Award.

Data availability

The data supporting the findings of this study are available from the corresponding author upon reasonable request.

References

1. Mills KT, Bundy JD, Kelly TN, Reed JE, Kearney PM, Reynolds K, Chen J, He J. Global disparities of hypertension prevalence and control: a systematic analysis of population-based studies from 90 countries. *Circulation* 2016;**134**:441–450.
2. Andersson C, Vasan RS. Epidemiology of heart failure with preserved ejection fraction. *Heart Fail Clin* 2014;**10**:377–388.
3. Ziaeian B, Fonarow GC. Epidemiology and aetiology of heart failure. *Nat Rev Cardiol* 2016;**13**:368–378.
4. Drazner MH. The progression of hypertensive heart disease. *Circulation* 2011;**123**:327–334.
5. MacDonald EA, Rose RA, Quinn TA. Neurohumoral control of sinoatrial node activity and heart rate: insight from experimental models and findings from humans. *Front Physiol* 2020;**11**:170.
6. Mangoni ME, Nargeot J. Genesis and regulation of the heart automaticity. *Physiol Rev* 2008;**88**:919–982.
7. Brubaker PH, Kitzman DW. Chronotropic incompetence: causes, consequences, and management. *Circulation* 2011;**123**:1010–1020.
8. Zweerink A, van der Lingen ACJ, Handoko ML, van Rossum AC, Allaart CP. Chronotropic incompetence in chronic heart failure. *Circ Heart Fail* 2018;**11**:e004969.
9. Borlaug BA, Melenovsky V, Russell SD, Kessler K, Pacak K, Becker LC, Kass DA. Impaired chronotropic and vasodilator reserves limit exercise capacity in patients with heart failure and a preserved ejection fraction. *Circulation* 2006;**114**:2138–2147.
10. Lakatta EG, Maltsev VA, Vinogradova TM. A coupled SYSTEM of intracellular Ca^{2+} clocks and surface membrane voltage clocks controls the timekeeping mechanism of the heart's pacemaker. *Circ Res* 2010;**106**:659–673.
11. Hua R, Adamczyk A, Robbins C, Ray G, Rose RA. Distinct patterns of constitutive phosphodiesterase activity in mouse sinoatrial node and atrial myocardium. *PLoS One* 2012;**7**:e47652.
12. Vinogradova TM, Kobrinsky E, Lakatta EG. Dual activation of phosphodiesterases 3 and 4 regulates basal spontaneous beating rate of cardiac pacemaker cells: role of compartmentalization? *Front Physiol* 2018;**9**:1301.
13. Xiang YK. Compartmentalization of beta-adrenergic signals in cardiomyocytes. *Circ Res* 2011;**109**:231–244.
14. Vinogradova TM, Sirenko S, Lukyanenko YO, Yang D, Tarasov KV, Lyashkov AE, Varghese NJ, Li Y, Chakir K, Ziman B, Lakatta EG. Basal spontaneous firing of rabbit sinoatrial node cells is regulated by dual activation of PDEs (phosphodiesterases) 3 and 4. *Circ Arrhythm Electrophysiol* 2018;**11**:e005896.
15. Richter W, Jin SL, Conti M. Splice variants of the cyclic nucleotide phosphodiesterase PDE4D are differentially expressed and regulated in rat tissue. *Biochem J* 2005;**388**:803–811.
16. Shi Q, Li M, Mika D, Fu Q, Kim S, Phan J, Shen A, Vandecasteele G, Xiang YK. Heterologous desensitization of cardiac beta-adrenergic signal via hormone-induced betaAR/arrestin/PDE4 complexes. *Cardiovasc Res* 2017;**113**:656–670.
17. Richter W, Day P, Agrawal R, Bruss MD, Granier S, Wang YL, Rasmussen SG, Horner K, Wang P, Lei T, Patterson AJ, Kobilka B, Conti M. Signaling from beta1- and beta2-adrenergic receptors is defined by differential interactions with PDE4. *EMBO J* 2008;**27**:384–393.
18. Xiang Y, Naro F, Zoudilova M, Jin SL, Conti M, Kobilka B. Phosphodiesterase 4D is required for beta2 adrenoceptor subtype-specific signaling in cardiac myocytes. *Proc Natl Acad Sci U S A* 2005;**102**:909–914.
19. Zaccolo M, Pozzan T. Discrete microdomains with high concentration of cAMP in stimulated rat neonatal cardiac myocytes. *Science* 2002;**295**:1711–1715.
20. Mesquita T, Zhang R, Cho JH, Zhang R, Lin YN, Sanchez L, Goldhaber JI, Yu JK, Liang JA, Liu W, Trayanova NA, Cingolani E. Mechanisms of sinoatrial node dysfunction in heart failure with preserved ejection fraction. *Circulation* 2022;**145**:45–60.
21. Sarma S, Stoller D, Hendrix J, Howden E, Lawley J, Livingston S, Adams-Huet B, Holmes C, Goldstein DS, Levine BD. Mechanisms of chronotropic incompetence in heart failure with preserved ejection fraction. *Circ Heart Fail* 2020;**13**:e006331.
22. Colucci WS, Ribeiro JP, Rocco MB, Quigg RJ, Creager MA, Marsh JD, Gauthier DF, Hartley LH. Impaired chronotropic response to exercise in patients with congestive heart failure. Role of postsynaptic beta-adrenergic desensitization. *Circulation* 1989;**80**:314–323.
23. Dorey TW, Moghtadaei M, Rose RA. Altered heart rate variability in angiotensin II-mediated hypertension is associated with impaired autonomic nervous system signaling and intrinsic sinoatrial node dysfunction. *Heart Rhythm* 2020;**17**:1360–1370.
24. Mackasey M, Egom EE, Jansen HJ, Hua R, Moghtadaei M, Liu Y, Kaur J, McRae MD, Bogachev O, Rafferty SA, Ray G, Kirkby AW, Rose RA. Natriuretic peptide receptor-C protects against angiotensin II-mediated sinoatrial node disease in mice. *JACC Basic Transl Sci* 2018;**3**:824–843.
25. Dorey TW, Mackasey M, Jansen HJ, McRae MD, Bohne LJ, Liu Y, Belke DD, Atkinson L, Rose RA. Natriuretic peptide receptor B maintains heart rate and sinoatrial node function via cyclic GMP-mediated signalling. *Cardiovasc Res* 2022;**118**:1917–1931.
26. Tuomi JM, Bohne LJ, Dorey TW, Jansen HJ, Liu Y, Jones DL, Rose RA. Distinct effects of ibrutinib and acalabrutinib on mouse atrial and sinoatrial node electrophysiology and arrhythmogenesis. *J Am Heart Assoc* 2021;**10**:e022369.
27. Jansen HJ, Mackasey M, Moghtadaei M, Belke DD, Egom EE, Tuomi JM, Rafferty SA, Kirkby AW, Rose RA. Distinct patterns of atrial electrical and structural remodeling in angiotensin II mediated atrial fibrillation. *J Mol Cell Cardiol* 2018;**124**:12–25.
28. Jansen HJ, Mackasey M, Moghtadaei M, Liu Y, Kaur J, Egom EE, Tuomi JM, Rafferty SA, Kirkby AW, Rose RA. NPR-C (natriuretic peptide receptor-C) modulates the progression of angiotensin II-mediated atrial fibrillation and atrial remodeling in mice. *Circ Arrhythm Electrophysiol* 2019;**12**:e006863.
29. Lang D, Petrov V, Lou Q, Osipov G, Efimov IR. Spatiotemporal control of heart rate in a rabbit heart. *J Electrocardiol* 2011;**44**:626–634.
30. Azer J, Hua R, Krishnaswamy PS, Rose RA. Effects of natriuretic peptides on electrical conduction in the sinoatrial node and atrial myocardium of the heart. *J Physiol* 2014;**592**:1025–1045.
31. Post SR, Hammond HK, Insel PA. Beta-adrenergic receptors and receptor signaling in heart failure. *Annu Rev Pharmacol Toxicol* 1999;**39**:343–360.
32. Bender AT, Beavo JA. Cyclic nucleotide phosphodiesterases: molecular regulation to clinical use. *Pharmacol Rev* 2006;**58**:488–520.
33. Tsukamoto Y, Mano T, Sakata Y, Ohtani T, Takeda Y, Tamaki S, Omori Y, Ikeya Y, Saito Y, Ishii R, Higashimori M, Kaneko M, Miwa T, Yamamoto K, Komuro I. A novel heart failure mice model of hypertensive heart disease by angiotensin II infusion, nephrectomy, and salt loading. *Am J Physiol Heart Circ Physiol* 2013;**305**:H1658–H1667.
34. Crowley SD, Gurley SB, Herrera MJ, Ruiz P, Griffiths R, Kumar AP, Kim HS, Smithies O, Le TH, Coffman TM. Angiotensin II causes hypertension and cardiac hypertrophy through its receptors in the kidney. *Proc Natl Acad Sci U S A* 2006;**103**:17985–17990.
35. Andersen MJ, Borlaug BA. Heart failure with preserved ejection fraction: current understandings and challenges. *Curr Cardiol Rep* 2014;**16**:501.
36. Opie LH, Sack MN. Enhanced angiotensin II activity in heart failure: reevaluation of the counterregulatory hypothesis of receptor subtypes. *Circ Res* 2001;**88**:654–658.
37. Schnelle M, Catibog N, Zhang M, Nabeebaccus AA, Anderson G, Richards DA, Sawyer G, Zhang X, Toischer K, Hasenfuss G, Monaghan MJ, Shah AM. Echocardiographic evaluation of diastolic function in mouse models of heart disease. *J Mol Cell Cardiol* 2018;**114**:20–28.
38. Shin K, Shin K, Hong S. Heart rate recovery and chronotropic incompetence in patients with prehypertension. *Minerva Med* 2015;**106**:87–94.
39. Glukhov AV, Fedorov VV, Anderson ME, Mohler PJ, Efimov IR. Functional anatomy of the murine sinus node: high-resolution optical mapping of ankyrin-B heterozygous mice. *Am J Physiol Heart Circ Physiol* 2010;**299**:H482–H491.
40. Bloch Thomsen PE, Jons C, Raatikainen MJ, Moerch Joergensen R, Hartikainen J, Virtanen V, Boland J, Anttonen O, Gang UJ, Hoest N, Boersma LV, Platou ES, Becker D, Messier MD, Huikuri HV, Cardiac A; Risk Stratification After Acute Myocardial Infarction Study Group. Long-term recording of cardiac arrhythmias with an implantable cardiac monitor in patients with reduced ejection fraction after acute myocardial infarction: the Cardiac Arrhythmias and Risk Stratification After Acute Myocardial Infarction (CARISMA) study. *Circulation* 2010;**122**:1258–1264.
41. John RM, Kumar S. Sinus node and atrial arrhythmias. *Circulation* 2016;**133**:1892–1900.
42. DiFrancesco D. The role of the funny current in pacemaker activity. *Circ Res* 2010;**106**:434–446.

43. Zaza A, Robinson RB, DiFrancesco D. Basal responses of the L-type Ca^{2+} and hyperpolarization-activated currents to autonomic agonists in the rabbit sino-atrial node. *J Physiol* 1996;**491**:347–355.
44. Reddy GR, Ren L, Thai PN, Caldwell JL, Zaccolo M, Bossuyt J, Ripplinger CM, Xiang YK, Nieves-Cintron M, Chiamvimonvat N, Navedo MF. Deciphering cellular signals in adult mouse sinoatrial node cells. *iScience* 2022;**25**:103693.
45. de Lucia C, Eguchi A, Koch WJ. New insights in cardiac beta-adrenergic signaling during heart failure and aging. *Front Pharmacol* 2018;**9**:904.
46. Kokkonen K, Kass DA. Nanodomain regulation of cardiac cyclic nucleotide signaling by phosphodiesterases. *Annu Rev Pharmacol Toxicol* 2017;**57**:455–479.
47. Mika D, Richter W, Conti M. A CaMKII/PDE4D negative feedback regulates cAMP signaling. *Proc Natl Acad Sci U S A* 2015;**112**:2023–2028.
48. Perry SJ, Baillie GS, Kohout TA, McPhee I, Magiera MM, Ang KL, Miller WE, McLean AJ, Conti M, Houslay MD, Lefkowitz RJ. Targeting of cyclic AMP degradation to beta 2-adrenergic receptors by beta-arrestins. *Science* 2002;**298**:834–836.
49. Liu S, Li Y, Kim S, Fu Q, Parikh D, Sridhar B, Shi Q, Zhang X, Guan Y, Chen X, Xiang YK. Phosphodiesterases coordinate cAMP propagation induced by two stimulatory G protein-coupled receptors in hearts. *Proc Natl Acad Sci U S A* 2012;**109**:6578–6583.
50. Eschenhagen T. PDE4 in the human heart—major player or little helper? *Br J Pharmacol* 2013;**169**:524–527.
51. Molina CE, Leroy J, Richter W, Xie M, Scheitrum C, Lee IO, Maack C, Rucker-Martin C, Donzeau-Gouge P, Verde I, Llach A, Hove-Madsen L, Conti M, Vandecasteele G, Fischmeister R. Cyclic adenosine monophosphate phosphodiesterase type 4 protects against atrial arrhythmias. *J Am Coll Cardiol* 2012;**59**:2182–2190.
52. Molenaar P, Christ T, Hussain RI, Engel A, Berk E, Gillette KT, Chen L, Galindo-Tovar A, Krobert KA, Ravens U, Levy FO, Kaumann AJ. PDE3, but not PDE4, reduces beta1- and beta2-adrenoceptor-mediated inotropic and lusitropic effects in failing ventricle from metoprolol-treated patients. *Br J Pharmacol* 2013;**169**:528–538.
53. Richter W, Xie M, Scheitrum C, Krall J, Movsesian MA, Conti M. Conserved expression and functions of PDE4 in rodent and human heart. *Basic Res Cardiol* 2011;**106**:249–262.

Translational perspective

Chronotropic incompetence and impaired β-adrenergic receptor (β-AR) signalling are prevalent in hypertensive heart disease and heart failure leading to poor heart rate control and increased mortality. We report that impaired β-AR responsiveness in the sinoatrial node (SAN) in AngII-mediated hypertensive heart disease occurs due to increased activity of phosphodiesterase 4D (PDE4D) in the SAN. This results in impaired effects of β-AR agonists on SAN spontaneous action potential firing and SAN ionic currents (I_f and $I_{Ca,L}$). These data suggest that PDE4D could be a novel target for treating chronotropic incompetence in hypertensive heart disease.

PDE4D mediates impaired β-adrenergic receptor signaling in the sinoatrial node in mice with hypertensive heart disease

Supplemental Material

Supplemental Methods

Mice

Mice were housed in groups of 3-5 per cage using Tecniplast Green Line GM500 cages with 500 cm^2 of floor space and provided with enrichment items (nesting material, houses) in the cages. Mice were provided with standard rodent chow (LabDiet 5062) and water *ad libitum*. Mice were kept on a 12:12 hour light:dark cycle. Temperature in the room was maintained at 21-21.5°C and humidity was 32-38%. These environmental and housing conditions were monitored daily and maintained throughout all studies. All experimental procedures were approved by the University of Calgary Animal Care and Use Committee and were in accordance with the guidelines of the Canadian Council on Animal Care and the NIH guide for the care and use of laboratory animals. For surgeries and tissue isolations mice were anaesthetized using isoflurane (2%, inhalation). Mice were euthanized by cervical dislocation under isoflurane anaesthesia.

Telemetry

Telemetric ECG recordings (HD-X11 telemeters, Data Sciences International) were used to measure heart rate (HR) and locomotor activity levels in conscious freely moving mice. ECG leads were positioned subcutaneously in a lead II position to continuously measure HR. Activity was measured from telemeters as the relative movement of the mouse, which is dependent on the orientation and distance between the transmitter and receiver and quantified in counts per minute. Baseline ECG and activity data were collected for 36 hrs once a week for 3 weeks following surgery.

Segments where mice transitioned from low activity to high activity were identified based on activity measured from telemeters. Associated HRs for each segment were taken and averaged as a measure of the mouse's HR responsiveness to spontaneous activity. Low/high-activity phases were divided into 10 min episodes. Each episode was examined to ensure a stationary and stable sinus rhythm with no trend or periodic fluctuations. Next, R-wave detection was performed, and R-R interval time series were obtained. The time domain parameters reported include the standard deviation of all normal R–R intervals (SDNN, in ms) and the root mean square differences between successive R-R intervals (RMSSD, in ms).

Intrinsic HR was investigated weekly by combined intraperitoneal injection of the β-adrenergic receptor (β-AR) antagonist propranolol hydrochloride (10 mg/kg) and the muscarinic receptor antagonist atropine sulfate (10 mg/kg). ECG data acquisition, ECG filtering and R-wave detection was done using PowerLab and LabChart (ADInstruments, V8).

In-vivo electrophysiology

HR was measured in anesthetized mice (2% isoflurane inhalation) using 30-gauge subdermal needle electrodes (Grass Technologies) to record body surface (lead II) ECGs. Once a stable HR was obtained for 10 min, mice were injected subcutaneously with a bolus of the β-adrenergic receptor agonist isoproterenol (10mg/kg). ECG data acquisition, ECG filtering and R-wave detection was done using a dual Bio-amp connected to PowerLab and LabChart (ADInstruments, V8). Body temperature was monitored continuously via a rectal probe and maintained at 37°C with a heating pad.

Blood pressure

Blood pressure was measured in conscious restrained mice using a tail cuff apparatus (IITC Life Sci). Mice underwent 2 days of training where they were placed in the tail cuff apparatus without cuff placement or inflation to acclimatize in order to minimize the effect of

restraint stress on blood pressure measurements. Measurements were collected over 2 days and averaged together to ensure accurate readings. Mice were allowed 10 minutes to acclimate to the restraints prior to blood pressure measurements. All readings were performed in a quiet dark room at a similar time of day to further minimize stress and the effect of diurnal variation in blood pressure. Blood pressure measurements were analyzed using IITC Life Sci Blood Pressure Analysis software.

High-resolution optical mapping

To investigate patterns of electrical conduction in the SAN we used high resolution optical mapping in atrial preparations. Hearts were excised into Krebs solution (37°C) containing (in mM): 118 NaCl, 4.7 KCl, 1.2 KH_2PO_4, 25 $NaHCO_3$, 1 $CaCl_2$, 1 $MgCl_2$, 11 glucose and bubbled with 95% O_2/5% CO_2 to maintain a pH of 7.4. The atrial preparation was superfused continuously with Krebs solution (37°C) bubbled with 95% O_2/5% CO_2 and allowed to equilibrate for at least 30 min. The preparation was then incubated with the voltage-sensitive dye RH-237 (15 μM; Biotium) for 15 min. After the dye incubation period, superfusion was resumed with blebbistatin (10 μM; Cayman Chemical Company) added to the superfusate to suppress contractile activity and prevent motion artifacts. Experiments were performed in sinus rhythm so that the cycle length (i.e., beating rate) of the atrial preparation was free to change. RH-237-loaded atrial preparations were illuminated with light from the X-Cite Xylis Broad Spectrum LED Illumination System (Excelitas Technologies) and filtered with a 520/35 nm excitation filter (Semrock). Emitted fluorescence was separated by a dichroic mirror (560 nm cut-off; Semrock) and filtered by a 715 nm long-pass emissions filter (Andover Corp.). Recordings were captured using a high-speed CMOS camera (MiCAM03-N256, SciMedia). We mapped conduction in the region of the right atrial posterior wall around the point of initial electrical excitation, which corresponds to the activation of the SAN. The region that was mapped extended from the superior vena cava to the inferior cava along the edge of the crista terminalis, based on the

known anatomical location of the SAN in the mouse heart. Data were captured from an optical field of view of 6.8 x 6.8 mm at a frame rate of 3000 frames/s using BrainVision software (BrainVision Inc.). The spatial resolution was 37.6 x 37.6 μM for each pixel. Magnification was constant in all experiments and no pixel binning was used. All optical data were analyzed using custom software written in MATLAB® (Mathworks).

Patch clamping of sinoatrial node myocytes

Mice were administered a 0.2 ml intraperitoneal injection of heparin (1000 IU/ml) to prevent blood clotting. Following this, mice were anesthetized by isoflurane inhalation and then euthanized by cervical dislocation. The heart was excised into Tyrode's solution (35ºC) consisting of (in mmol/L) 140 NaCl, 5.4 KCl, 1.2 KH_2PO4, 1.0 $MgCl_2$, 1.8 $CaCl_2$, 5.55 glucose, and 5 HEPES, with pH adjusted to 7.4 with NaOH. The sinoatrial node (SAN) region of the heart was isolated by separating the atria from the ventricles, cutting open the superior and inferior venae cavae, and pinning the tissue so that the crista terminalis could be identified. The SAN area is located in the intercaval region adjacent to the crista terminalis. This SAN region was cut into strips, which were transferred and rinsed in a 'low Ca^{2+}, Mg^{2+} free' solution containing (in mmol/L) 140 NaCl, 5.4 KCl, 1.2 KH_2PO_4, 0.2 $CaCl_2$, 50 taurine, 18.5 glucose, 5 HEPES and 1 mg/ml bovine serum albumin (BSA), with pH adjusted to 6.9 with NaOH. SAN tissue strips were digested in 5 ml of 'low Ca^{2+}, Mg^{2+} free' solution containing collagenase (type II, Worthington Biochemical 4 Corporation), elastase (Worthington Biochemical Corporation) and protease (type XIV, Sigma Chemical Company) for 30 min. Then the tissue was transferred to 5 ml of modified KB solution containing (in mmol/L) 100 potassium glutamate, 10 potassium aspartate, 25 KCl, 10 KH_2PO_4, 2 $MgSO_4$, 20 taurine, 5 creatine, 0.5 EGTA, 20 glucose, 5 HEPES, and 0.1% BSA, with pH adjusted to 7.2 with KOH. The tissue was mechanically agitated using a wide-bore pipette. This procedure yielded individual SAN myocytes with cellular automaticity that was recovered after readapting the cells to a physiological concentration of Ca^{2+}. SAN myocytes

were identified by their small spindle shape and ability to beat spontaneously in the recording chamber when superfused with normal Tyrode's solution. When patch-clamped, SAN myocytes displayed spontaneous action potentials and the hyperpolarization-activated current, I_f. The capacitance of single SAN myocytes was 20–44 pF. In AAV9 experiments, only GFP+ SAN myocytes (Figure 7A) were used for patch clamp studies.

Spontaneous action potentials (APs) were recorded using the perforated patch-clamp technique on single SAN cells. I_f, and $I_{Ca,L}$ were recorded by voltage clamping single SAN using the patch-clamp technique in the whole cell configuration. APs and membrane currents were recorded at room temperature (22-23 °C). For recording APs and I_f the recording chamber was superfused with a normal Tyrode's solution containing (in mmol/L) 140 NaCl, 5 KCl, 1 $MgCl_2$, 1 $CaCl_2$, 10 HEPES, and 5 glucose, with pH adjusted to 7.4 with NaOH. The pipette filling solution for APs and I_f contained (in mmol/L) 135 KCl, 0.1 $CaCl_2$, 1 $MgCl_2$, 5 NaCl, 10 EGTA, 4 Mg-ATP, 6.6 Na-phosphocreatine, 0.3 Na-GTP and 10 HEPES, with pH adjusted to 7.2 with KOH. Amphotericin B (200 µg/ml) was added to this pipette solution to record APs with the perforated patch clamp technique. $BaCl_2$ (1×10^{-4} mol/L) was added to the superfusate when recording I_f, in order to eliminate any inward rectifier K^+ current that could be present at low levels in some SAN myocytes. For recording $I_{Ca,L}$ SAN myocytes were superfused with a modified Tyrode's solution containing the following (in mmol/L) 140 TEA-Cl, 5.4 CsCl, 2 $CaCl_2$, 1 $MgCl_2$, 10 HEPES, and 5 glucose with pH adjusted to 7.4 with CsOH. The pipette solution for $I_{Ca,L}$ contained (in mmol/L) 135 CsCl, 0.2 $CaCl_2$, 1 $MgCl_2$, 5 NaCl, 5 EGTA, 4 Mg-ATP, 6.6 Naphosphocreatine, 0.3 Na-GTP and 10 HEPES, with pH adjusted to 7.2 with CsOH.

Micropipettes were pulled from borosilicate glass (with filament, 1.5 mm OD, 0.75 mm ID, Sutter Instrument Company) using a Flaming/Brown pipette puller (model p-87, Sutter Instrument Company). The resistance of these pipettes was 4–8MΩ when filled with recording solution. Micropipettes were positioned with a micromanipulator (Burleigh PCS-5000 system) mounted on the stage of an inverted microscope (Olympus IX71). Seal resistance was 2–15

GΩ. Rupturing the sarcolemma in the patch for voltage clamp experiments resulted in access resistances of 5–15MΩ. Series resistance compensation averaged 80–85% using an Axopatch 200B amplifier (Molecular Devices). For perforated patch clamp experiments, access resistance was monitored for the development of capacitative transients upon sealing to the cell membrane with amphotericin B in the pipette. Typically, access resistance became less than 30MΩ within 5 min of sealing onto the cell, which was sufficient for recording spontaneous APs in current clamp mode. Data were digitized using a Digidata 1440 and pCLAMP 10 software (Molecular Devices) and stored on computer for post hoc analysis. Spontaneous AP parameters, including the maximum diastolic potential (MDP), the slope of the diastolic depolarization (DD slope), the maximum AP upstroke velocity (V_{max}), the AP overshoot and the AP duration at 50% repolarization (APD_{50}) were analyzed. The DD slope was measured by fitting a straight line to the linear portion of this AP component.

I_f was recorded from a holding potential of -35 mV. Voltage clamp steps (2 s duration) between -140 mV and -30 mV, followed by a voltage clamp step (1 s duration) to -130 mV, were used to measure total I_f current at each membrane potential as well as the tail current at -130 mV. Activation kinetics for I_f were determined by normalizing tail currents at each voltage to the maximum current level at -130 mV and fitting the data to the Boltzmann function: $I/Imax=1/(1+exp[(V_m-V_{1/2})/k])$ where V_m is the potential of the voltage clamp step, $V_{1/2}$ is the voltage at which 50% activation occurs and k is the slope factor.

$I_{Ca,L}$ was recorded from a holding potential of -80 mV. Following a prepulse to -60 mV to inactivate T-type Ca^{2+} channels, voltage clamp steps (200 ms in duration) between -80 mV and 60 mV were used to record total $I_{Ca,L}$ (i.e. $Ca_V1.3$ and $Ca_V1.2$ dependent $I_{Ca,L}$) at each membrane potential. $I_{Ca,L}$ activation kinetics were determined by calculating chord conductance (G) with the equation $G=I/(V_m-E_{rev})$, where V_m represents the depolarizing voltages and E_{rev} is the reversal potential estimated from the current-voltage relation of $I_{Ca,L}$. Maximum conductance

(G_{max}) and $V_{1/2}$ of activation for $I_{Ca,L}$ was determined using the following function: $G=[(V_m-V_{rev})][G_{max}][-1/[(1+\exp((V_m-V_{1/2})/k))+1]]$.

Ca^{2+} imaging

SAN myocytes were isolated as described above. Cells were plated in a stimulation chamber (Warner) for 30 minutes in KB solution containing 1µg/ml Fluo-4 AM (Molecular Probes). After perfusing the cells for 5 minutes with Tyrode's solution, spontaneous Ca^{2+} activity was captured using a Zeiss Axiocam 702 mono camera on a Zeiss Axio Observer microscope equipped with a pE340 fura light source (illuminating for Ex340, Ex380 and white light 435-645nm) and filter set for Fluo-4 (Ex470/40, Em525/50, Dic495). Ca2+ fluorescence was first recorded in control conditions when perfused with normal Tyrode's solution and then again in the presence of 10 nM isoproterenol. Data were analyzed using imageJ and a customized MATLAB software to quantify Ca^{2+} transient (CaT) parameters including amplitude, rise time and 70% decay time (T_{70}).

cAMP assay

cAMP levels were measured from live cells. Two mouse SAN myocyte isolations were performed as described above, pooled together to ensure adequate cell number, and centrifuged (2000 rpm) for 10 minutes. The supernatant was removed, and the pellet was resuspended in normal Tyrode's solution. A hemocytometer was used to determine myocyte density. Cells were incubated with either Tyrode's solution (untreated control) or isoproterenol (10 µM) for 15 min at room temperature (21°C). Intracellular cAMP concentrations were then determined using a HTRF cAMP Femto2 kit (Cisbio US, kit #62AM4PEB) according to the manufacturer's instructions and normalized to myocyte density.

Phosphodiesterase activity assay

Phosphodiesterase activity was assessed in SAN tissue. Two SAN samples were pooled together and homogenized in non-denaturing lysis buffer (20 mM Tris HCl, 137 mM NaCl, 1% Nonident P-40, 2 mM EDTA) and Protease Inhibitor Cocktail (Sigma-Aldrich) and PhosSTOP™ (Roche) to ensure adequate protein concentration. Tissue homogenates were then desalted using Zeba Spin Desalting Columns (ThermoFisher Scientific). Protein concentration was measured as described above. Phosphodiesterase activity was then measured using the Phosphodiesterase Activity Assay Kit (Abcam, kit#ab13946) as per the manufacturer's instructions. The activity of PDE4 was quantified as the difference between baseline 5'-AMP (pmol) produced after 60 minutes and the amount produced in the presence of the PDE4 inhibitor rolipram (10 μM). Final activity was standardized to sample protein concentration and represented as 5'-AMP (pmol/mg protein/min).

Quantitative PCR

PCR primers (Integrated DNA Technologies) were designed for *Pde4a* (PDE4A), *Pde4b* (PDE4B), and *Pde4d* (PDE4D) and *Pde3a* (PDE3A). GAPDH was used as the reference gene. Primer sequences are provided in Supplemental Table S9. Following synthesis, primers were reconstituted in nuclease free water at a concentration of 100 μM and stored at -20°C. All primer sets were validated in order to determine optimal annealing temperature as well as confirmation of ideal amplification efficiency (between 90-110% copy efficiency per cycle). RNA was extracted in PureZOL™ RNA isolation reagent according to kit instructions (Aurum Total RNA Fatty and Fibrous Tissue Kit, Bio-Rad). RNA was eluted in 40 μl of elution buffer from the spin column. RNA purity and quantity were determined using a NanoDrop ND-1000 spectrophotometer (NanoDrop Technologies, Wilmington, DE, USA). First strand synthesis reactions were performed using the iScript cDNA synthesis kit (Bio-Rad) according to kit instructions. Lack of genomic DNA contamination was verified by reverse transcription (RT)-

PCR using a no RT control. RT-qPCR using BRYT green dye (Promega) was used to assess gene expression.

Western blotting

Protein samples were extracted from two SANs and pooled for each experimental replicate in order to ensure sufficient protein. Tissues were pre-cooled in liquid nitrogen and homogenized in an ice-cold RIPA buffer (50 mM Tris, 150 mM NaCl, 1 mM EDTA, 25 mM sucrose, 1% Triton, 0.1% SDS) containing 0.5 mM DTT (1,4-Dithiothreitol, Roche) and Protease Inhibitor Cocktail (SigmaAldrich). Preparation was centrifuged at 10000rpm at 4ºC for 10mins. Protein concentrations were measured using a Bio-Rad DC™ Protein Assay Kit II (Bio-Rad). Protein samples (25 µg/lane) were separated by 12% SDS-polyacrylamide gels (SDS-PAGE) and transferred onto Biotrace™ NT nitrocellulose Transfer Membrane (VWR). The membrane was blocked with 1% casein in tris-buffered saline (TBS; Bio-Rad) for 1 hour and incubated overnight at 4ºC with rabbit primary antibodies ((PDE4D 1:500, PDE3A 1:500 β_1-AR 1:500, β_2-AR 1:500, GAPDH 1:5000, Abcam). The membrane was washed 3 times with TBST (TBS with 1% Tween 20 (Bio-Rad)) and incubated with goat anti-rabbit IgG coupled to horseradish peroxidase (HRP; Abcam) at 1:20000 for 1 hour at room temperature. Then the membrane was washed again 3 times with TBST. ECL (Bio-Rad) was added, incubated for 5 min and the membrane was scanned using the ChemiDoc system (Bio-Rad). We quantified expression of each of these proteins based on the identification of bands at the predicted molecular according to the information from the supplier. In some cases total protein was measured using a Mini-PROTEAN TGX stain-free gel (BioRad) according to manufacturer's instructions..

Co-immunoprecipitation

Two SAN samples were pooled together and homogenized in non-denaturing lysis buffer (20 mM Tris HCl, 137 mM NaCl, 1% Nonident P-40, 2 mM EDTA) and Protease Inhibitor

Cocktail (Sigma-Aldrich) and PhosSTOP™ (Roche) to ensure adequate protein concentration. Extracts were then precleared with 20 µl of A/G agarose beads (ThermoFisher Scientific) for 1 hour, followed by centrifugation at 10000 RPM at 4°C for 10 min. Supernatants from the precleared extracts were then immunoprecipitated using 10 µg of β_1-AR or β_2-AR antibody overnight at 4°C. Incubated supernatants were spun down at 10000 RPM at 4°C for 10 min and washed 3x with lysis buffer to minimize non-specific co-immunoprecipitation complexes. Finally, protein complexes were eluted from the beads using 1x sample buffer and loaded for SDS-PAGE as described above.

Immunocytochemistry

SAN myocytes were isolated as described above. Cells were added to an 8 Well Poly-L-Lysine coated plate (Ibidi) and given 1 hour to adhere. Cells were then fixed in 10% formalin for 10 minutes at 4° and washed in 1X PBS (Gibco) for 15 minutes. 1% Triton X-100 (1:100; Sigma-Aldrich) was added and left for 10 minutes followed by a 10 min wash with 1X PBS. Cells were then blocked with 15% goat serum (Gibco) for 1 hr and then incubated with the appropriate combination of the following primary antibodies: Goat anti-β_2-AR (1:100; ThermoFisher Scientific) or Goat anti-β_1-AR (1:100; Abcam) with Rabbit anti-PDE4d (1:100, Abcam) overnight at 4°C. Cells were then incubated with Alexa Fluor 488 Goat anti-Rabbit IgG (H+L; Invitrogen) and Alexa Fluor Plus 647 Donkey anti-Goat (H+L; Invitrogen) or Alexa Fluor Plus 555 Donkey anti-Goat (H+L; Invitrogen) secondary antibody at a dilution of 1:100 for 1 hour in a light protected container at room temperature. Cells were then washed 3 times for 5 minutes each and stored in 1X PBS. Negative controls were perfromed to confirm absence of non-specific staining. Images were acquired by confocal microscopy on a Leica SP8 LIGHTING microscoe equipped with a 63X objective. Following acquisition, fluorescence intensity and colocalization

(Pearson's coefficient) were quantified using ImageJ (NIH) to assess the degree of β_1-AR:PDE4D and β_2-AR:PDE4D colocalization.

Adeno-associated viral knockdown

Recombinant AAV9 vectors containing an shRNA for murine PDE4D under the U6 promoter (AAV9-GFP-U6-m-PDE4D-shRNA) were obtained from Vector BioLabs (Malvern PA). AAV9 vectors expressing a scrambled PDE4D shRNA sequence under the U6 promoter (AAV9-GFP-U6-scramble-shRNA) served as one of the negative controls, while another group was injected with saline (Supplemental Figure S3). AAV9 constructs also expressed GFP under the CMV promoter. For Ca^{2+} imaging studies with PDE4D knockdown, GFP was replaced with mCherry in the AAV9 construct to avoid overlap with fluo-4 fluorescence. Initially, two doses of virus ($1x10^{10}$ and $1.5x10^{11}$) were tested by retro-orbital injection in 8-10-week-old mice under anesthetic (2% isoflurane). The dose of $1.5x10^{11}$ genomic copies resulted in more consistent and effective infection of the heart and was used in all studies (Supplemental Figure S4). Mice were allowed 2 weeks for recovery and to ensure systemic viral delivery before undergoing mini-osmotic pump insertions as described above.

AAV9-GFP-U6-m-PDE4D-shRNA sequence:
(5'-CACCGCAGACTTGCGAAGCGAATCACTCGAGTGATTCGCTTCGCAAGTCTGCTTTTT-3')

AAV9-GFP-U6-scramble-shRNA sequence:
(5'-CCTAAGGTTAAGTCGCCCTCGCTCGAGCGAGGGCGACTTAACCTTAGG-3')

Supplemental Figures

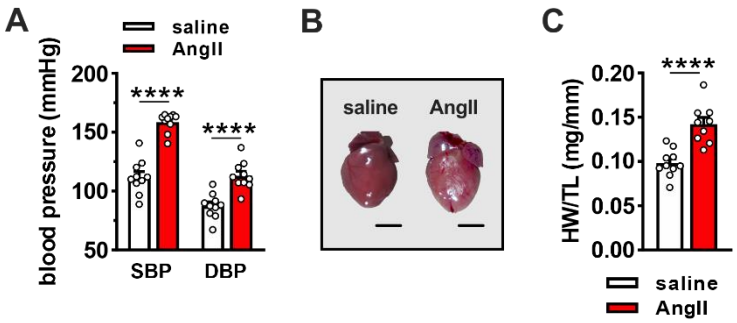

Figure S1: AngII induces hypertensive heart disease in mice. (**A**) Systolic and diastolic blood pressure (SBP and DBP) after 3 weeks of saline (*n*=10) and AngII (*n*=10) infusion. (**B**) Representative images of hearts from saline and AngII-infused mice demonstrating cardiac hypertrophy and atrial enlargement following 3 weeks of AngII infusion. (**C**) Summary of heart weight/tibia length (HW/TL) measurements in saline (*n*=10) and AngII (*n*=9) infused mice. Panels **A** and **C** analyzed by Student's *t*-test.

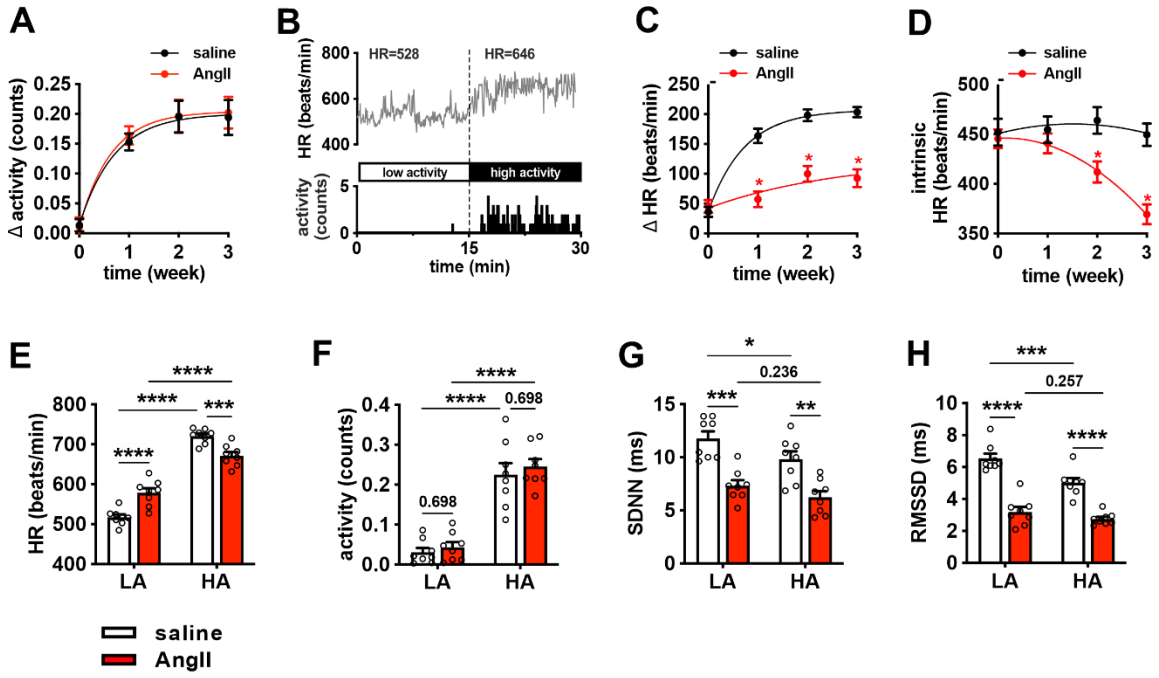

Figure S2: Heart rate and heart rate variability in conscious mice during AngII infusion. (**A**) Summary of change (Δ) in activity level during three weeks of saline or AngII infusion in conscious mice. (**B**) Representative tachogram demonstrating changes in heart rate as a function of activity level in conscious mice. (**C**) Summary of changes in HR (Δ HR) in response to increasing activity levels in conscious saline and AngII-infused mice. (**D**) Summary of intrinsic heart rate (HR), measured during autonomic nervous system blockade, in conscious saline and AngII-infused mice. (**E-H**) Summary of heart rate (HR; **E**), activity (**F**), SDNN (**G**) and RMSSD (**H**) during low and high activity after 3 weeks of saline or AngII infusion. Data analyzed by two-way repeated measures ANOVA with Holm-Sidak posthoc test; *n*=8 saline and 8 AngII infused mice.

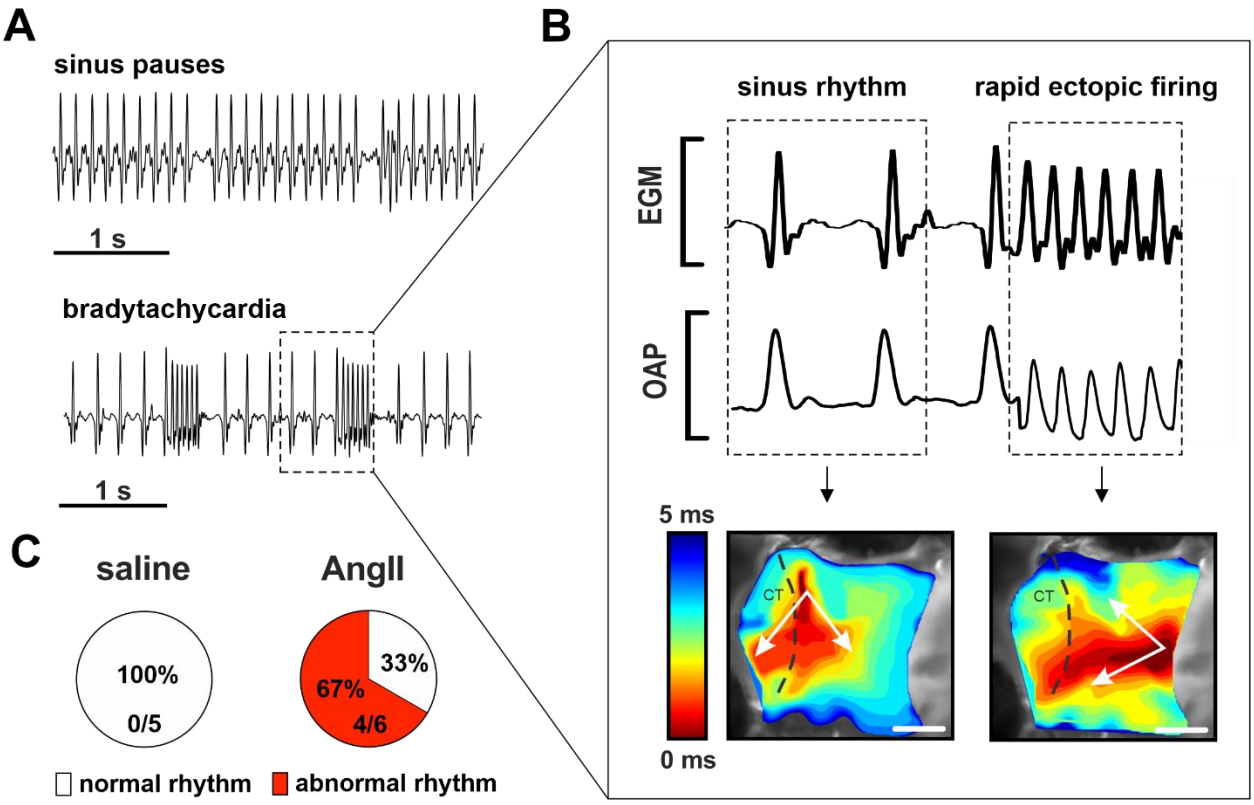

Figure S3: Arrhythmogenesis in AngII infused mice during β-AR stimulation.
(**A**) Representative arrhythmias and summary of abnormal rhythms seen in atrial preparations from saline and AngII-infused mice in the presence of ISO. (**B**) Callout of brady-tachy rhythm captured with high resolution optical mapping of the right atrial posterior wall in an AngII heart. Electrogram (EGM) and optical action potentials demonstrate normal activations in sinus rhythm followed by rapid firing. Corresponding activation maps show that rapid activations originated from an ectopic site in the inter-atrial septum. (**C**) Summary of the number of atrial preparations that exhibited abnormal rhythms following β-AR stimulation in saline (*n*=5) and AngII (*n*=6) infused mice. For panel **C,** *P*=0.06 by Fisher's exact test.

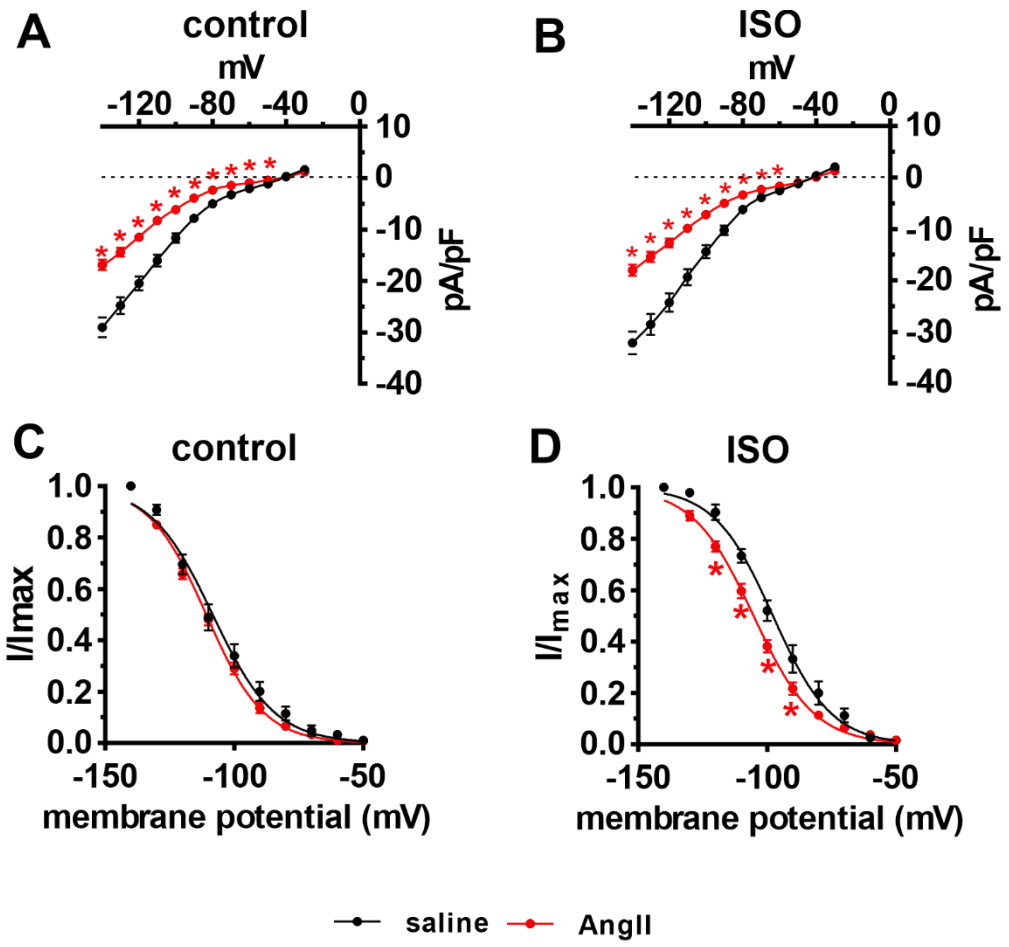

Figure S4: I_f IV curves and steady-state activation curves in SAN myocytes from AngII infused mice. (A-B) I_f IV curves in control conditions (**A**) and after superfusion of ISO (10 nM) (**B**) in isolated SAN myocytes from saline and AngII infused mice. (**C-D**) I_f steady-state activation curves in control conditions (**C**) and after superfusion of ISO (**D**) in isolated SAN myocytes from saline and AngII-infused mice. *n*=7 cells from 4 mice for saline 10 cells from 7 mice for AngII. Data analyzed by two-way repeated measures ANOVA with Holm-Sidak posthoc test.

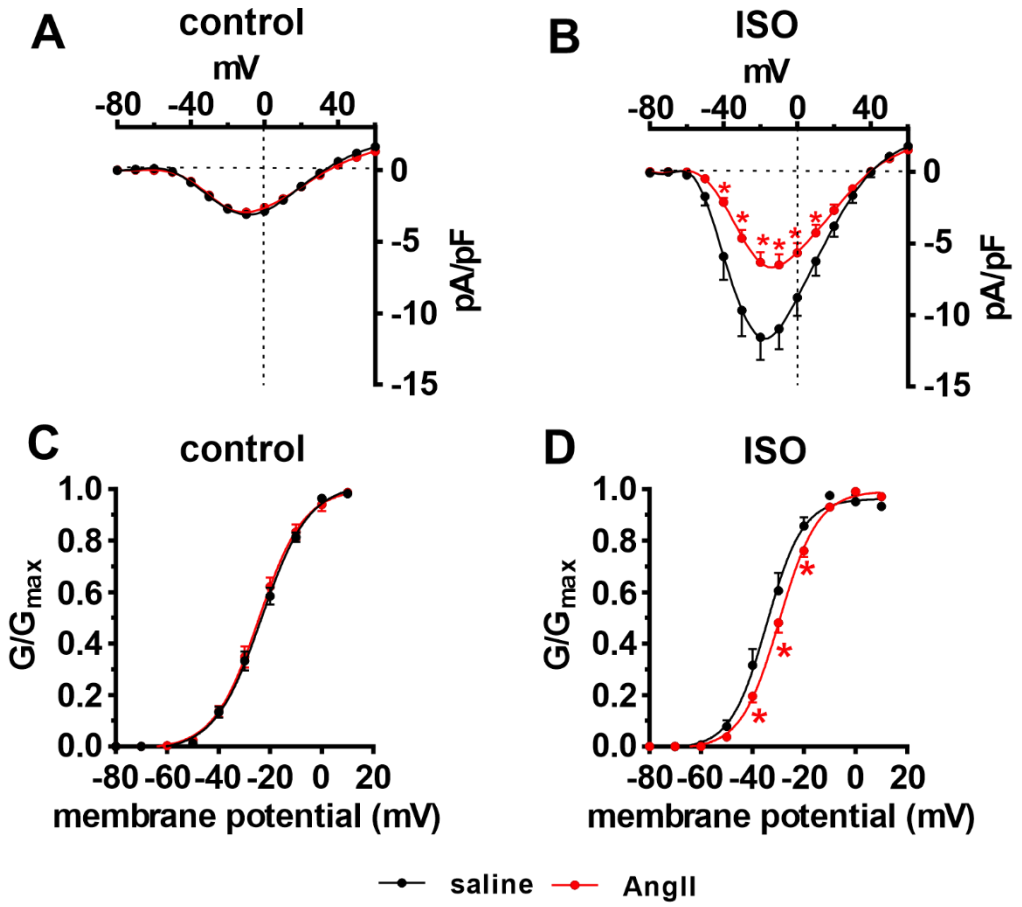

Figure S5: $I_{Ca,L}$ IV curves and steady-state activation curves in SAN myocytes from AngII-infused mice. (A-B) $I_{Ca,L}$ IV curves in control conditions (**A**) and after superfusion of ISO (10 nM) (**B**) in isolated SAN myocytes from saline and AngII infused mice. (**C-D**) $I_{Ca,L}$ steady-state activation curves in control conditions (**C**) and after superfusion of ISO (**D**) in isolated SAN myocytes from saline and AngII-infused mice. *n*=9 cells from 4 mice for saline 8 cells from 5 mice for AngII. Data analyzed by two-way repeated measures ANOVA with Holm-Sidak posthoc test.

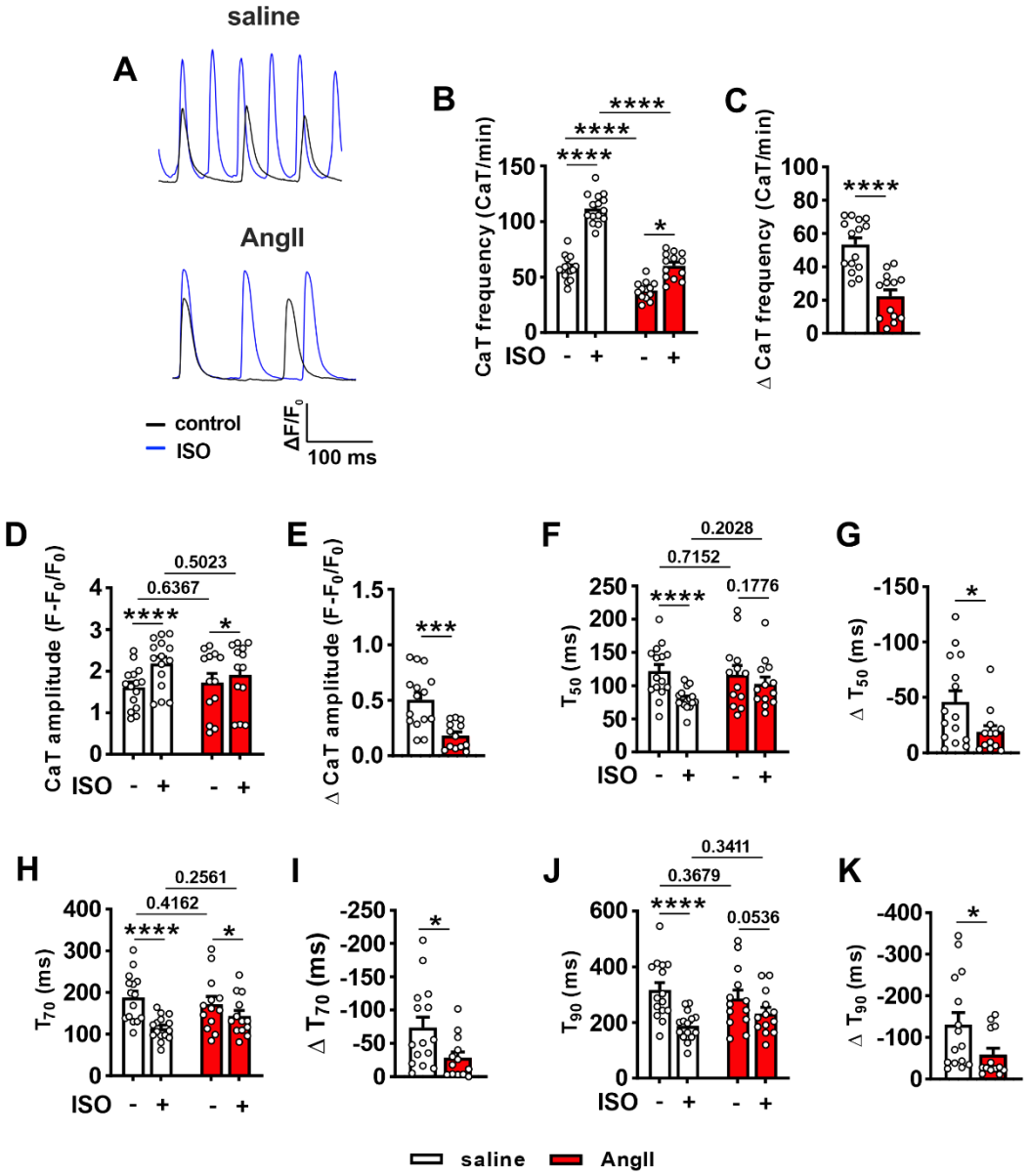

Figure S6: Effects of β-AR stimulation on SAN myocyte Ca^{2+} transient morphology in saline and AngII-infused mice. (**A**) Representative Ca^{2+} transients in control conditions and after superfusion of ISO (10 nM) in saline and AngII-infused mice. (**B-C**) CaT frequency in control conditions and after application of ISO (**B**) and the change in CaT frequency after application of ISO (**C**). (**D-E**) CaT amplitude in control conditions and after application of ISO (**D**) and the change in CaT amplitude after application of ISO (**E**). (**F-K)** CaT 50% decay time (T_{50}), T_{70}, and T_{90} in control conditions and after application of ISO (panels F, H, and J) and the change in CaT T_{50}, T_{70}, and T_{90} after application of ISO (panes G, I, and K) in saline and AngII-infused mice. *n*=15 cells from 3 mice for saline and 13 cells from 3 mice for AngII. Data in panels B, D, F, H and J analyzed by two-way repeated measures ANOVA with Holm-Sidak posthoc test. Data in panels C, E, G, I, and K analyzed by Student's *t*-test.

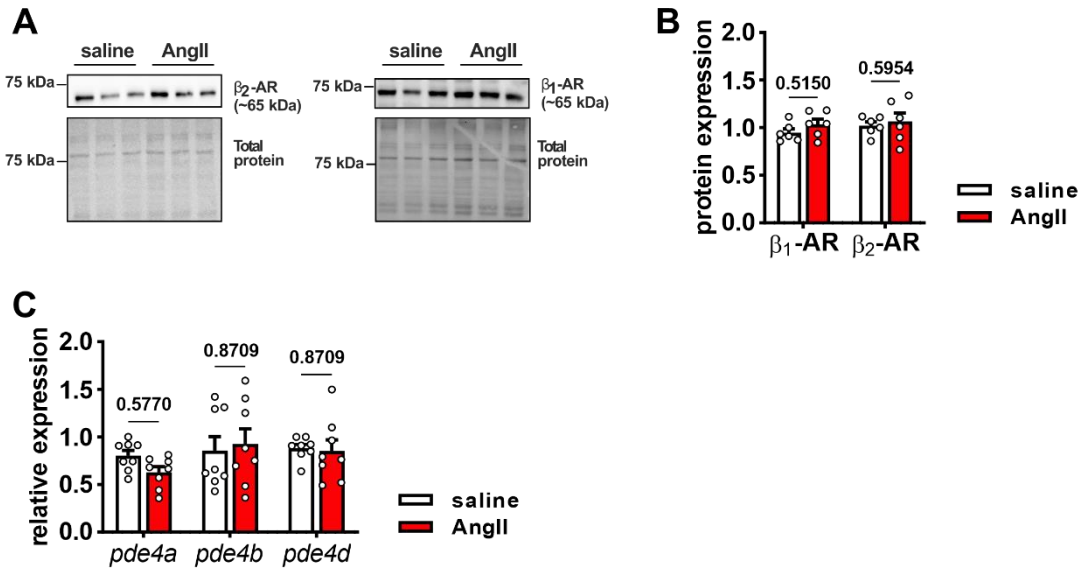

Figure S7: Protein expression of β-ARs and mRNA expression of PDE4 subtypes in the SAN in saline and AngII-infused mice. (**A-B**) Representative Western blots (**A**) and summary protein expression (**B**) for β_1 and β_2-ARs in the SAN in saline (*n*=6 pooled SANs) and AngII (*n*=6 pooled SANs) mice. (**C**) summary of mRNA expression of *pde4a*, *pde4b*, and *pde4d* in the SAN in saline (*n*=6 pooled SANs) and AngII (*n*=8 pooled SANs) mice. Summary data analyzed by two-way ANOVA with Holm-Sidak posthoc test. Uncropped blots provided in Figure S15.

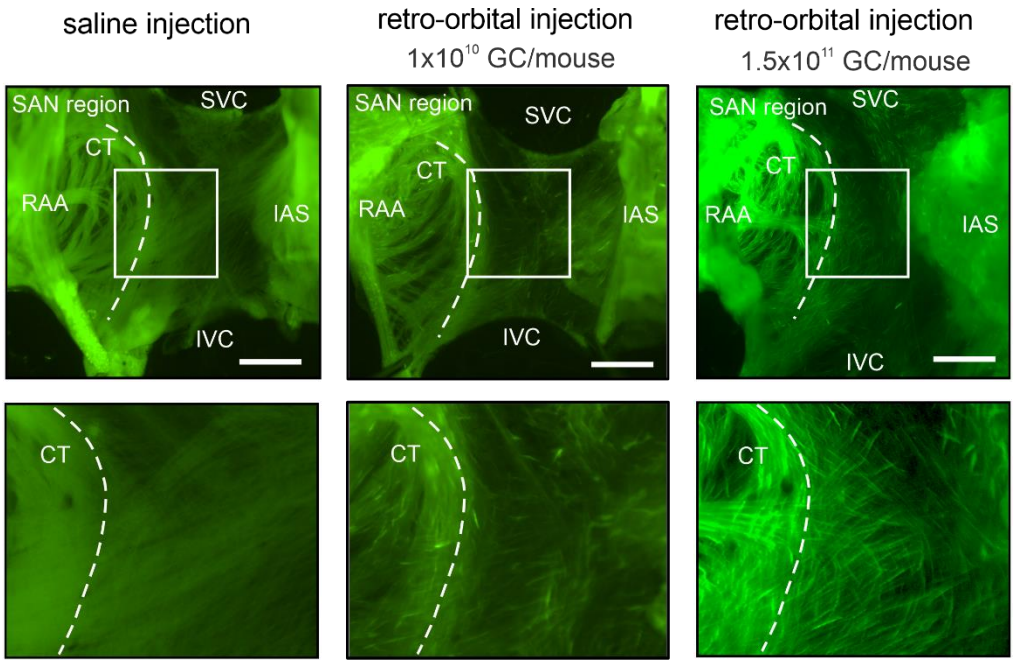

Figure S8: AAV9-mediated expression of GFP in the right atrial posterior wall.
Representative atrial preparations from mice injected retro-orbitally with either saline or AAV9-GFP at two different doses. Images show that $1.5x10^{11}$ genomic copies per mouse (GC/mouse) yielded high infection of the heart including throughout the posterior wall adjacent to the crista terminalis (CT), which corresponds to the SAN. The dose of $1.5x10^{11}$ was therefore used in all functional studies.

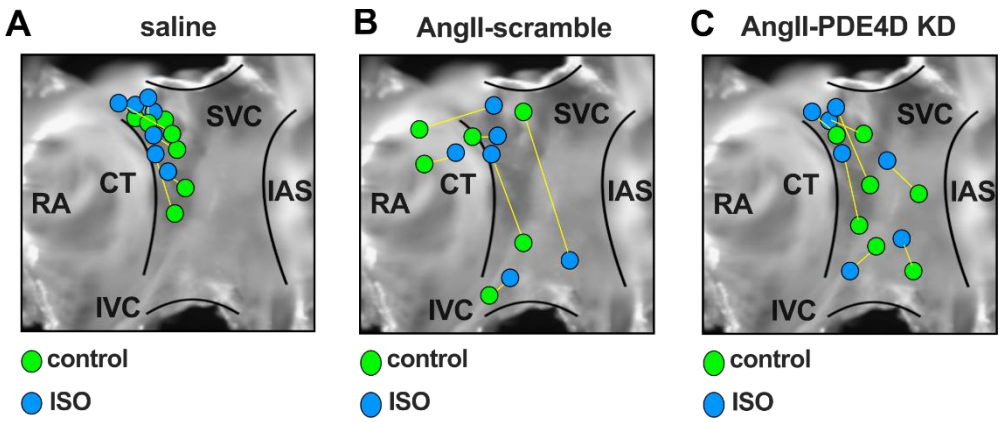

Figure S9: Effect of PDE4D knockdown on SAN initial activation sites. Initial activation sites in saline, AngII-scramble, and AngII-PDE4D KD hearts before (control) and after superfusion of ISO (10 nM). RA, right atrium; SVC, superior vena cava; IVC, inferior vena cava; IAS, interatrial septum.

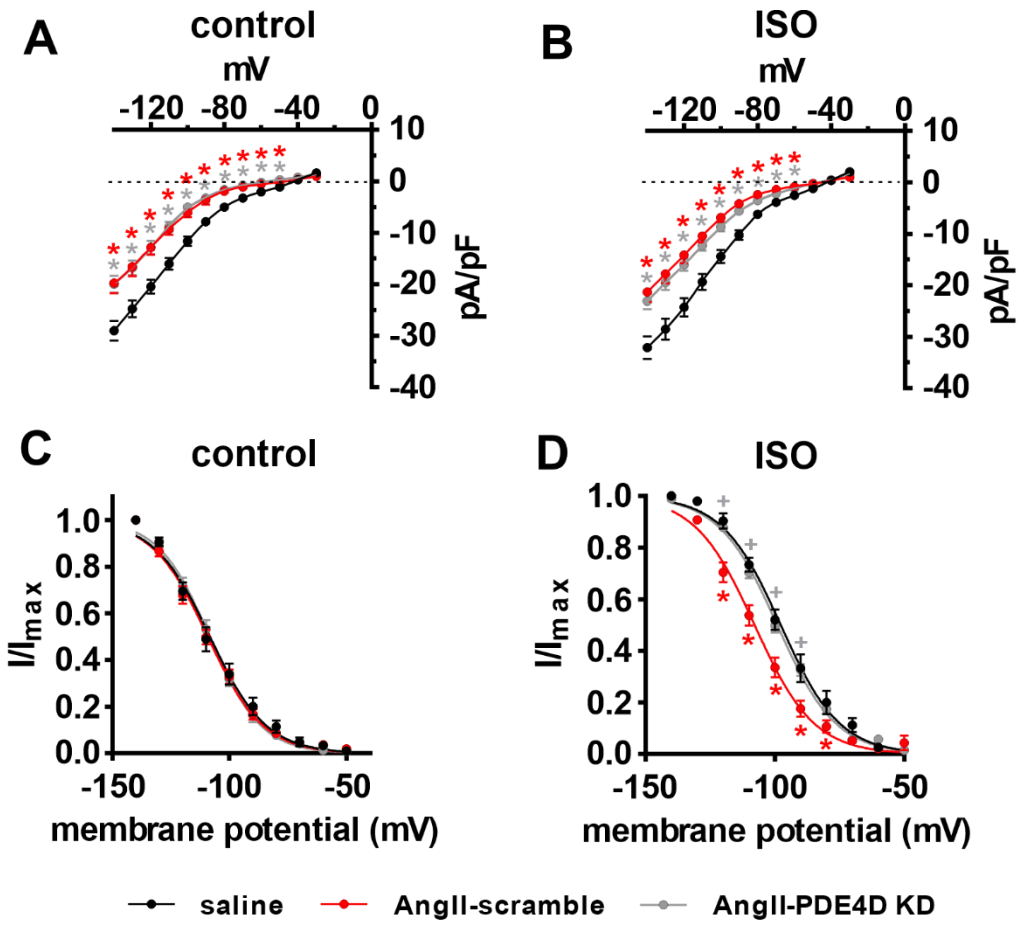

Figure S10: I_f IV curves and steady-state activation curves after PDE4D knockdown in SAN myocytes from AngII-infused mice. (A-B) I_f IV curves in control conditions (**A**) and after superfusion of ISO (10 nM) (**B**) in isolated SAN myocytes from saline, AngII-scramble, and AngII-PDE4D KD mice. (**C-D**) I_f steady-state activation curves in control conditions (**C**) and after superfusion of ISO (10 nM) (**D**) in isolated SAN myocytes from saline, AngII-scramble, and AngII-PDE4D KD mice. *n*=7 cells from 4 mice for saline, 6 cells from 3 mice for AngII-scramble, and 7 cells from 3 mice for AngII-PDE4D KD. Data analyzed by two-way repeated measures ANOVA with Holm-Sidak posthoc test.

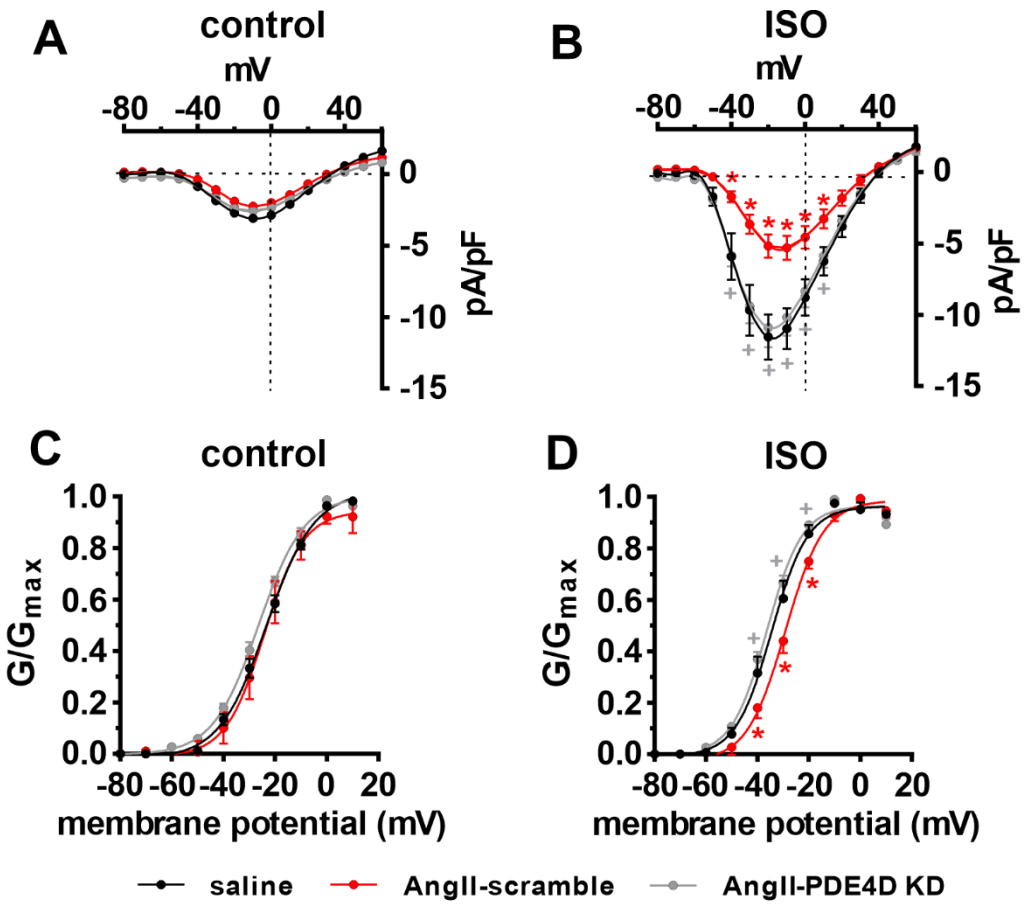

Figure S11: $I_{Ca,L}$ IV curves and steady-state activation curves after PDE4D knockdown in SAN myocytes from AngII-infused mice. (A-B) $I_{Ca,L}$ IV curves in control conditions (**A**) and after superfusion of ISO (10 nM) (**B**) in isolated SAN myocytes from saline, AngII-scramble, and AngII-PDE4D KD mice. (**C-D**) $I_{Ca,L}$ steady-state activation curves in control conditions (**C**) and after superfusion of ISO (10 nM) (**D**) in isolated SAN myocytes from saline, AngII-scramble, and AngII-PDE4D KD mice. *n*=9 cells from 4 mice for saline, 6 cells from 3 mice for AngII-scramble, and 7 cells from 3 mice for AngII-PDE4D KD. Data analyzed by two-way repeated measures ANOVA with Holm-Sidak posthoc test.

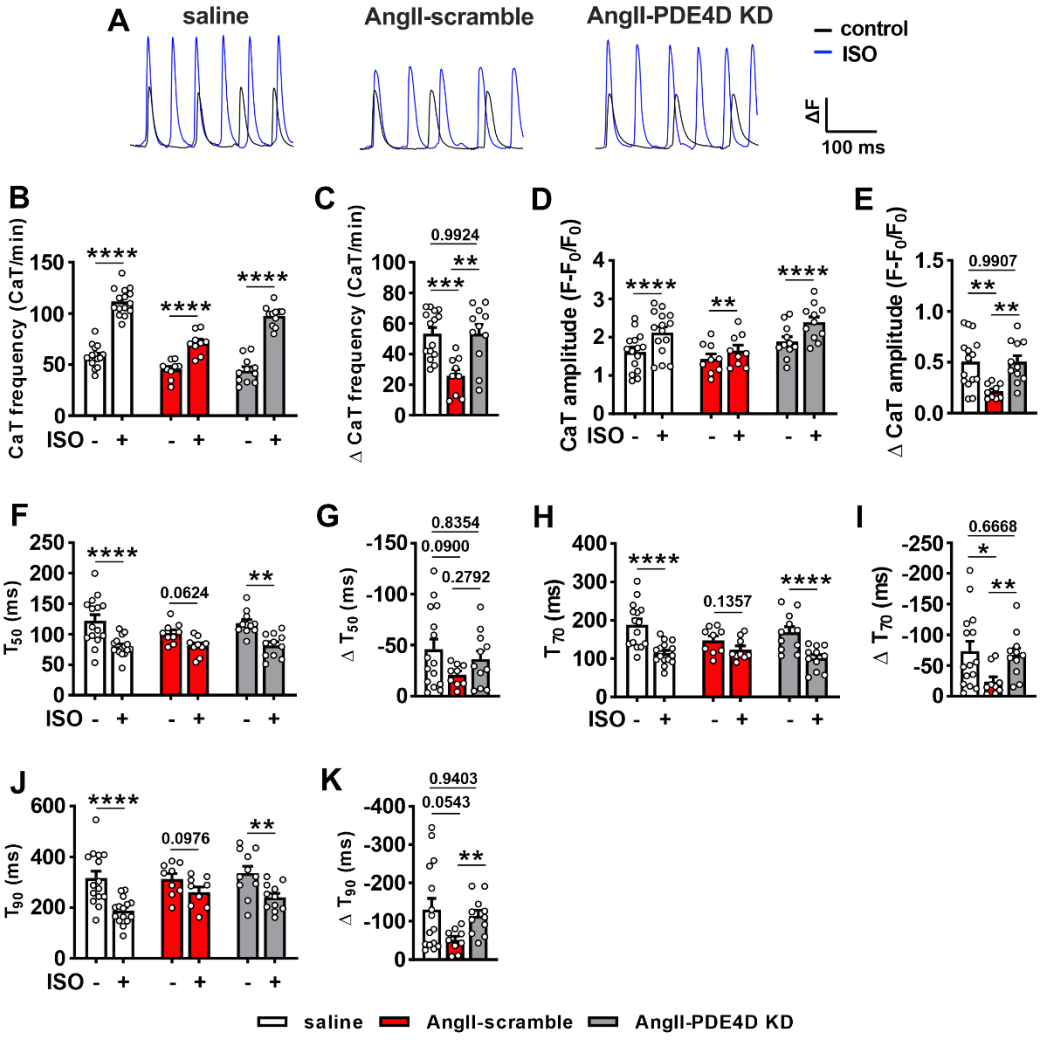

Figure S12: PDE4D knockdown normalizes the effects of ISO on Ca^{2+} transient morphology in isolated SAN myocytes from AngII-infused mice. (**A**) Representative Ca^{2+} transients in isolated SAN myocytes from saline, AngII-scramble, and AngII-PDE4D KD mice in control conditions and after superfusion of ISO (10 nM). (**B-C**) CaT frequency in control conditions and after application of ISO (**B**) and change in CaT frequency after ISO (**C**). (**D-E**) CaT amplitude in control conditions and after application of ISO (**D**) and change in CaT amplitude after ISO (**E**) in saline, AngII-scramble, and AngII-PDE4D KD SAN myocytes. (F-K) CaT 50% decay time (T_{50}), T_{70}, and T_{90} in control conditions and after application of ISO (panels F, H, and J) and the change in CaT T_{50}, T_{70}, and T_{90} after application of ISO (panes G, I, and K) in saline, AngII-scramble, and AngII-PDE4D KD SAN myocytes. *n*=15 cells from 3 mice for saline, 9 cells from 3 mice for AngII-scramble, and 11 cells from 3 mice for AngII-PDE4D KD. Data in panels B, D, F, H, and J analyzed by two-way repeated measures ANOVA with Holm-Sidak posthoc test. Data in panels C, E, G, I, and K analyzed by one-way ANOVA with Holm-Sidak posthoc test.

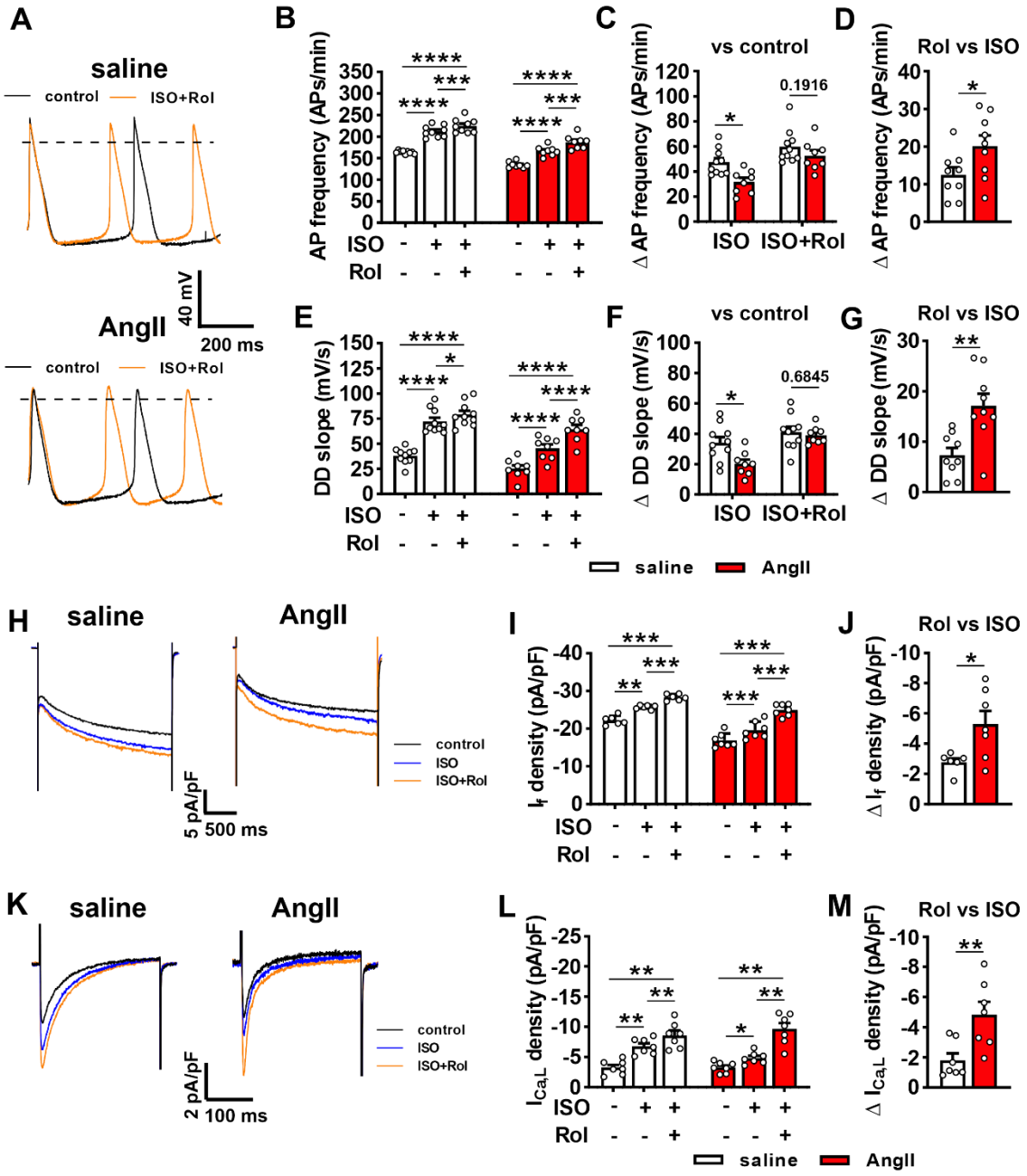

Figure S13: PDE4 inhibition increases β-AR responsiveness in isolated SAN myocytes from AngII-infused mice. (**A**) Representative spontaneous APs in isolated SAN myocytes from saline and AngII-infused mice in control conditions and after superfusion of ISO (10 nM) and the PDE4 inhibitor rolipram (Rol; 10 µM). (**B-G**) Summary data and Δ values for the effects of ISO and Rol on AP firing frequency (**B-D**) and DD slope (**E-G**) in SAN myocytes from saline (*n*=10 cells from 5 mice) and AngII-infused (*n*=8 cells from 4 mice) mice. (**H**) Representative I_f recordings (measured at -140 mV) in control conditions and after sequential application of ISO and ISO+Rol. (**I-J**) Summary of the effects of ISO and Rol on I_f density at -140 mV (**I**) and Δ I_f after ISO+Rol (**J**) in SAN myocytes from saline (*n*=6 cells from 3 mice) and AngII-infused (*n*=7

cells from 3 mice) infused mice. (**K**) Representative $I_{Ca,L}$ recordings (measured at -10 mV) in control conditions and after sequential application of ISO and ISO+Rol. (**L-M**) Summary of the effects of ISO and Rol on $I_{Ca,L}$ density at -10 mV (**L**) and Δ $I_{Ca,L}$ after ISO+Rol (**M**) in SAN myocytes from saline (*n*=7 cells from 3 mice) and AngII-infused (*n*=7 cells from 4 mice) infused mice. Panels B, C, E, F, I, and L analyzed by two-way repeated measures ANOVA with Holm-Sidak posthoc test. Panels D, G, J, and M analyzed by Student's *t*-test.

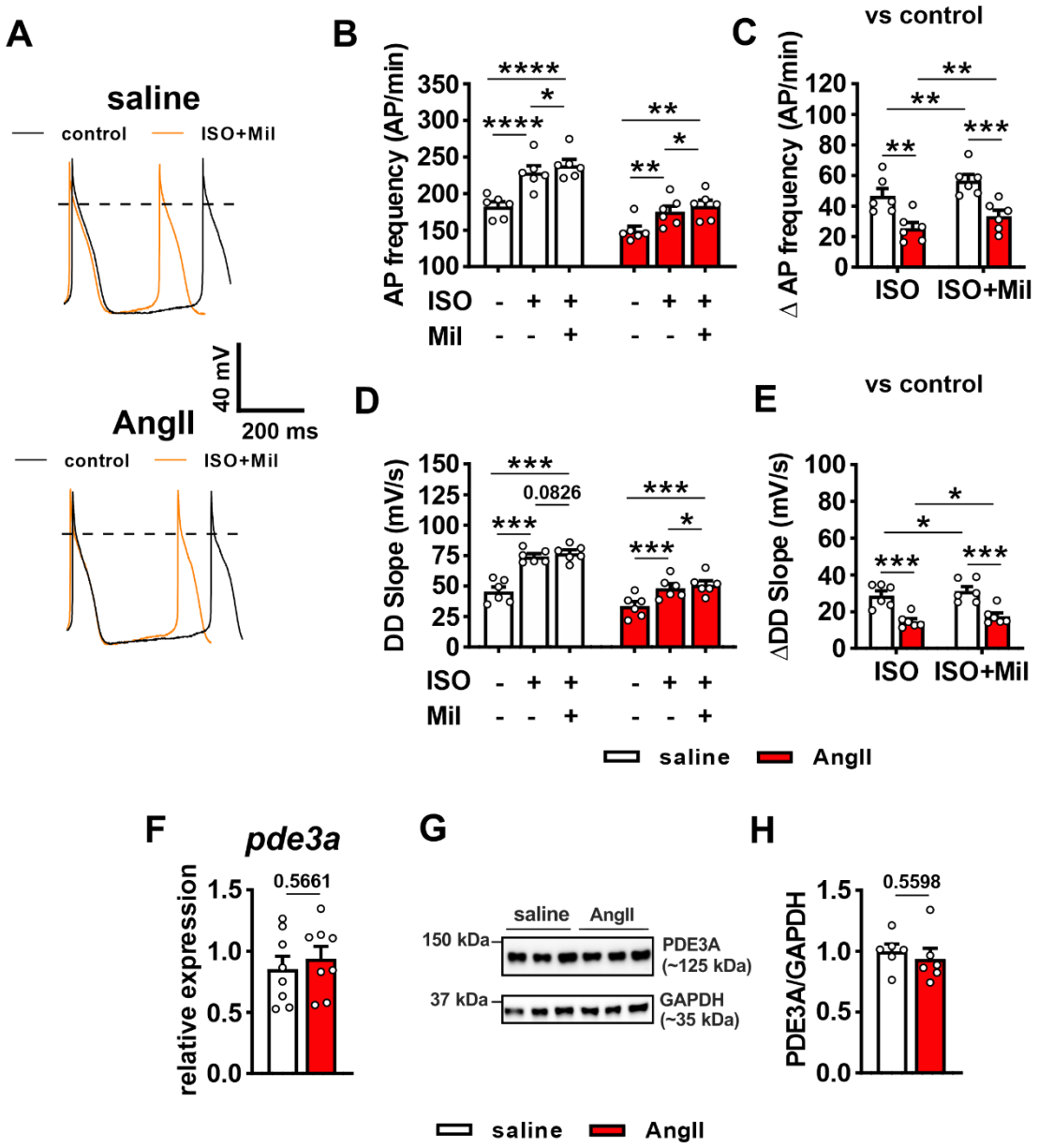

Figure S14: Effects of PDE3 inhibition on β-AR responsiveness in isolated SAN myocytes from AngII-infused mice. (A) Representative spontaneous APs in isolated SAN myocytes from saline and AngII-infused mice in control conditions and after superfusion of ISO (10 nM) and milrinone (Mil, 10 µM). (**B-E**) Summary data and Δ values for the effects of ISO and Mil on AP firing frequency (**B-C**) and DD slope (**D-E**) in SAN myocytes from saline (*n*=7 cells from 3 mice) and AngII-infused (*n*=6 cells from 3 mice) mice. Data analyzed by two-way repeated measures ANOVA with Holm-Sidak posthoc test. (**F**) *pde3a* mRNA expression in the SAN in saline (*n*=8 pooled SAN) and AngII-infused (*n*=8 pooled SAN) mice. (**G-H**) Representative Western blot (**G**) and summary of PDE3A protein expression (**H**) in the SAN of saline (*n*=6 pooled SAN) and AngII-infused (*n*=6 pooled SAN). Data in panels F and H analyzed by Student's *t*-test. Uncropped Western blot provided in Figure S13.

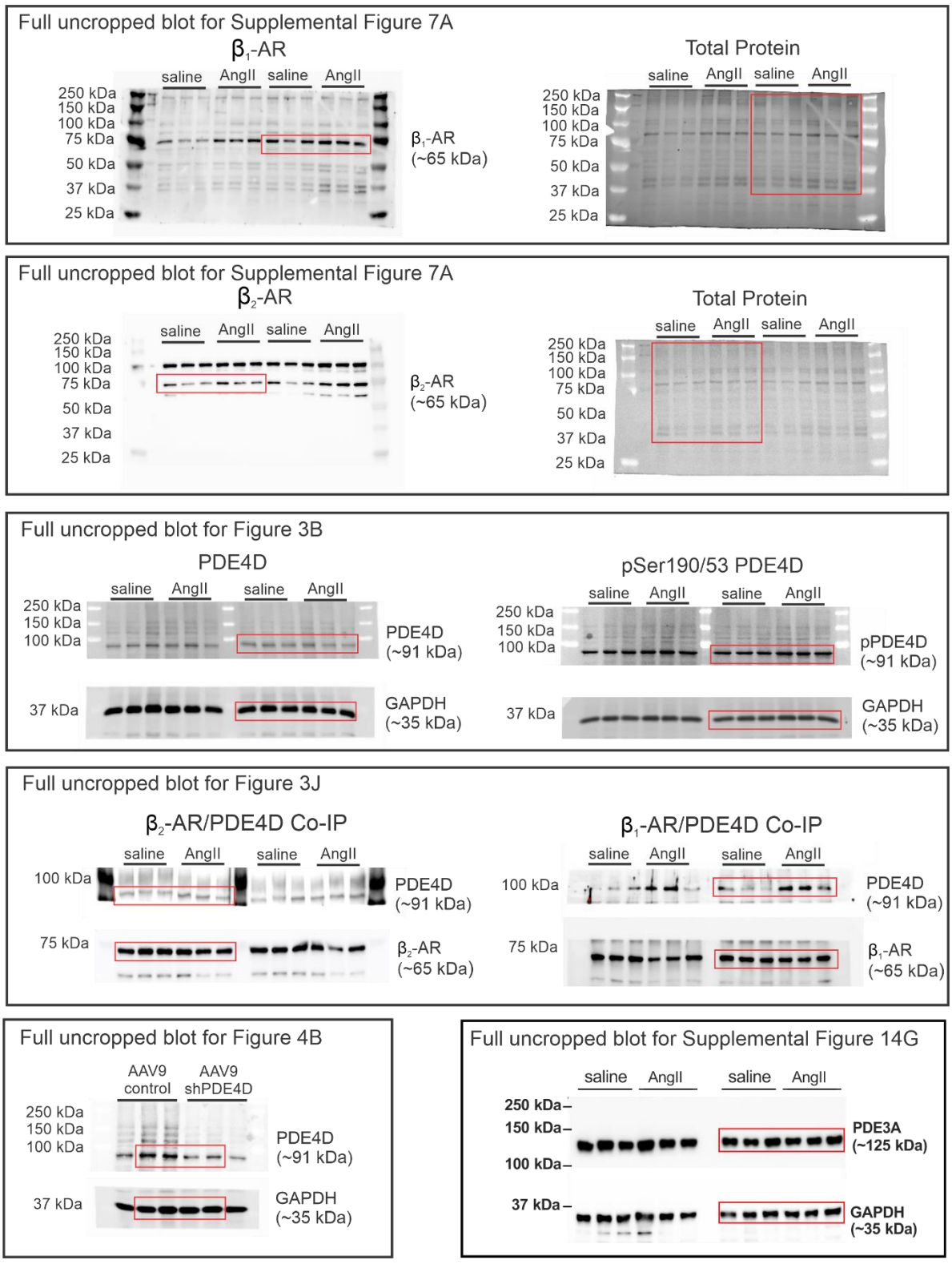

Figure S15: Full uncropped gels for Western blots.

Supplemental Tables

Table S1: Echocardiography measurements at baseline and after 3 weeks of infusion of saline or AngII.

	baseline		3 weeks	
	saline	**AngII**	**saline**	**AngII**
N	5	5	7	7
EF (%)	49.1±2.3	44.3±1.4	46.6±2.9	43.6±2.9
FS (%)	24.8±1.4	21.8±0.8	23.4±1.7	21.5±1.6
LVAWs (mm)	1.28±0.05	1.16±0.03	1.24±0.02	**1.33±0.03***†
LVAWd (mm)	0.87±0.04	0.82±0.02	0.88±0.03	**0.96±0.02***†
LVPWs (mm)	1.05±0.07	0.99±0.02	1.03±0.04	**1.15±0.04***†
LVPWd (mm)	0.76±0.05	0.75±0.03	0.8±0.02	**0.91±0.03***†
LVIDs (mm)	3.5±0.1	3.4±0.05	3.5±0.1	**2.5±0.1***†
LVIDd (mm)	4.6±0.09	4.4±0.05	4.5±0.1	**3.4±0.1***†
LA area$_{max}$ (mm^2)	5.71±0.3	5.04±0.26	5.87±0.65	**8.1±1.04***†
LA area$_{min}$ (mm^2)	3.02±0.45	2.86±0.31	3.23±0.44	**6.69±0.83***†
RA area$_{max}$ (mm^2)	3.93±0.96	3.33±0.51	4.16±0.79	**5.79±0.69***†
RA area$_{min}$ (mm^2)	2.98±0.43	3.46±0.91	2.73±0.39	**5.34±1.07***†

EF: ejection fraction, FS; fractional shortening, LVAW; left ventricular anterior wall thickness, LVPW; left ventricular posterior wall thickness; LVID, left ventricular internal diameter. LVAW, LVPW, and LVID measurements are shown during diastole (d) and systole (s). LA; left atrial, RA; right atrial. Data are means ± SEM; $^{*}P<0.05$ vs. saline, $^{\dagger}P<0.05$ vs baseline by mixed-effects ANOVA with Holm-Sidak posthoc test.

Table S2: Spontaneous AP parameters in SAN myocytes from saline- and AngII-infused mice in response to isoproterenol (ISO; 10 nM).

	control		ISO (10 nM)	
	saline	**AngII**	**saline**	**AngII**
***n* (*N*)**	12(6)	15(7)	-	-
Capacitance (pF)	37.4±1.3	36.9±1.4	-	-
Cycle length (ms)	363.7±6.3	**461.1±13.2***	**274.6±6.9†**	**378.8±10.7*†**
AP frequency (APs/min)	165.6±3.3	**131.6±3.7***	**220.1±5.9†**	**159.9±4.1*†**
MDP (mV)	-67.2±1.6	-65.7±0.9	-67.4±1.5	-66.4±0.9
DD Slope (mV/s)	38.8±2.1	**25.9±1.9***	**71.9±3.4†**	**44.9±3.8*†**
V_{max} (V/s)	85.1±11.9	75.6±0.9	82.9±10.1	72.7±9.1
OS (mV)	29.3±4.1	26.8±2.6	29.5±3.8	22.7±2.3
APD_{50} (ms)	37.3±2.5	41.9±2.5	**44.2±3.1†**	**49.1±4.5†**

n, cell sample size; *N*, mouse sample size; MDP, maximum diastolic potential; DD slope, diastolic depolarization slope; V_{max}, maximum AP upstroke velocity; OS, overshoot; APD_{50}, AP duration at 50% repolarization; Data are means ± SEM; **P*<0.05 vs. saline, †*P*<0.05 vs control by two-way repeated measures ANOVA with Holm-Sidak posthoc test.

Table S3: I_f peak density and activation kinetics.

	control		ISO (10 nM)	
	saline	**AngII**	**saline**	**AngII**
***n* (*N*)**	7(4)	10(7)	-	-
I_f at -70 mV (pA/pF)	-3.2±0.5	**-1.2±0.2***	**-4.9±0.4†**	**-1.9±0.2*†**
$V_{1/2(Act)}$ (mV)	-108.1±1.8	-110.6±0.9	**-96.9±1.7†**	**-104.8±1.2*†**
k (mV)	11.5±0.6	11.2±0.3	11.3±0.3	11.8±0.4

n, cell sample size; *N*, mouse sample size; $V_{1/2(Act)}$, voltage at which 50% of channels are activated; k, slope factor. Data are means ± SEM; **P*<0.05 vs. saline, †*P*<0.05 vs control by two-way repeated measures ANOVA with Holm-Sidak posthoc test.

Table S4: $I_{Ca,L}$ peak density and activation kinetics.

	control		ISO (10 nM)	
	saline	**AngII**	**saline**	**AngII**
***n* (*N*)**	9(4)	8(5)	-	-
$I_{Ca,L}$ at -10 mV (pA/pF)	-3.2±0.2	-2.9±0.2	**-10.2±1.3†**	**-6.5±0.7*†**
G_{max} (pS/pF)	72.2±4.6	74.4±5.1	**180.2±21.4†**	**129.2±15.6*†**
$V_{1/2(Act)}$ (mV)	-26.1±1.5	-26.4±2.2	**-36.0±5.4†**	**-30.3±1.2*†**
k (mV)	7.8±0.3	7.6±0.3	**5.4±0.3†**	**6.4±0.4*†**

n, cell sample size; *N*, mouse sample size; G_{max}, maximum conductance; $V_{1/2(Act)}$, voltage at which 50% of channels are activated; k, slope factor. Data are means ± SEM; **P*<0.05 vs. saline, †*P*<0.05 vs control by two-way repeated measures ANOVA with Holm-Sidak posthoc test.

Table S5: Spontaneous AP parameters in SAN myocytes from AAV9-scramble and PDE4D knockdown mice in response to isoproterenol (ISO; 10 nM).

	control		ISO (10 nM)	
	scramble	**PDE4D KD**	**scramble**	**PDE4D KD**
***n* (*N*)**	8(3)	12(3)	-	-
Capacitance (pF)	33.5±1.7	36.5±2.1	-	-
Cycle length (ms)	372.2±10.4	372.1±13.1	**294.8±5.4†**	**260.3±6.2*†**
AP frequency (APs/min)	162.1±4.5	163.2±5.1	**204.1±3.6†**	**232.6±6.2*†**
MDP (mV)	-65.5±0.8	-66.2±0.7	-65.3±0.8	-66.2±0.7
DD Slope (mV/s)	42.1±3.2	42.2±2.7	**67.0±3.2†**	**96.7±4.3*†**
V_{max} (V/s)	65.8±9.9	55.2±7.4	61.5±9.9	47.8±5.8
OS (mV)	26.6±6.1	19.1±4.1	22.8±3.9	14.0±2.5
APD_{50} (ms)	33.9±2.6	31.1±2.2	**46.6±2.9†**	**47.7±3.1†**

n, cell sample size; *N*, mouse sample size; MDP, maximum diastolic potential; DD slope, diastolic depolarization slope; V_{max}, maximum AP upstroke velocity; OS, overshoot; APD_{50}, AP duration at 50% repolarization; Data are means ± SEM; **P*<0.05 vs. scramble, †*P*<0.05 vs control by two-way repeated measures ANOVA with Holm-Sidak posthoc test.

Table S6: Spontaneous AP parameters in SAN myocytes from saline, AngII-scramble, and AngII-PDE4D KD mice in response to isoproterenol (ISO; 10 nM).

	control			ISO (10 nM)		
	saline	**AngII-scramble**	**AngII-PDE4D KD**	**saline**	**AngII-scramble**	**AngII-PDE4D KD**
***n* (*N*)**	12(6)	5(3)	6(3)	-	-	-
Capacitance (pF)	37.4±1.3	37.6±4.1	35.6±3.1	-	-	-
Cycle length (ms)	363.7±6.3	**574.1±17.6***	**462±27.4*#**	**274.6±6.9†**	**443.4±17.9*†**	**330.2±10.4#†**
AP frequency (APs/min)	165.6±3.3	**104.9±3.2***	**132.4±8.9*#**	**220.1±5.9†**	**136.2±5.5*†**	**182.6±6.3#†**
MDP (mV)	-67.2±1.6	-68.1±1.1	-67.3±1.9	-67.4±1.5	-69.3±0.8	-66.6±2.1
DD Slope (mV/s)	38.8±2.1	**20.1±2.1***	**30.6±1.6*#**	**71.9±3.4†**	**31.3±.1.9*†**	**57.3±2.7#†**
V_{max} (V/s)	85.1±11.9	75.4±6.2	68.3±10.3	82.9±10.1	71.7±8.2	67.2±7.2
OS (mV)	29.3±4.1	30.3±4.1	23.3±4.7	29.5±3.8	23.2±4.7	29.5±4.7
APD_{50} (ms)	37.3±2.5	36.7±4.7	41.1±2.8	**44.2±3.1†**	**44.1±5.1†**	**50.5±1.6†**

n, cell sample size; *N*, mouse sample size; MDP, maximum diastolic potential; DD slope, diastolic depolarization slope; V_{max}, maximum AP upstroke velocity; OS, overshoot; APD_{50}, AP duration at 50% repolarization; Data are means ± SEM; **P*<0.05 vs. saline, †*P*<0.05 vs. control, #*P*<0.05 vs. AngII-scramble by two-way repeated measures ANOVA with Holm-Sidak posthoc test.

Table S7: I_f activation kinetics in saline, AngII-scramble, and AngII-PDE4D-KD mice

	control			ISO (10 nM)		
	saline	**AngII-scramble**	**AngII-PDE4D-KD**	**saline**	**AngII-scramble**	**AngII-PDE4D-KD**
***n* (*N*)**	7(4)	6(3)	7(3)	-	-	-
I_f at -70 mV (pA/pF)	-3.2±0.5	**-1.1±0.3***	**-0.8±0.1***	**-4.9±0.4†**	**-1.7±0.4*†**	**-3.0±0.3*†**
$V_{1/2(Act)}$ (mV)	-108.1±1.8	-109.3±1.3	-108.4±1.7	**-96.9±1.7†**	**107.8±1.2*†**	**-98.1±1.1#†**
k (mV)	11.5±0.6	11.8±0.4	10.9±0.7	11.3±0.3	11.5±0.5	11.3±0.6

n, cell sample size; *N*, mouse sample size; $V_{1/2(Act)}$, voltage at which 50% of channels are activated; k, slope factor. Data are means ± SEM; **P*<0.05 vs. saline, †*P*<0.05 vs. control, #*P*<0.05 vs. AngII-scramble by two-way repeated measures ANOVA with Holm-Sidak posthoc test.

Table S8: $I_{Ca,L}$ activation kinetics in saline, AngII-scramble, and AngII-PDE4D-KD mice

	control			ISO (10 nM)		
	saline	**AngII-scramble**	**AngII-PDE4D-KD**	**saline**	**AngII-scramble**	**AngII-PDE4D-KD**
***n* (*N*)**	9(4)	6(3)	7(3)	-	-	-
$I_{Ca,L}$ at -10 mV (pA/pF)	-3.2±0.2	-2.2±0.3	-2.5±0.2	**-10.2±1.3†**	**-5.3±0.8*†**	**-10.2±1.3#†**
G_{max} (pS/pF)	72.2±4.6	69.5±12.1	71.7±4.2	**180.2±21.4†**	**108.2±14.6*†**	**177.8±21.3**
$V_{1/2(Act)}$ (mV)	-26.1±1.5	-23.4±1.7	-26.5±0.9	**-36.0±5.4†**	**-29.9±1.4*†**	**-36.9±0.9#†**
k (mV)	7.8±0.3	7.2±0.9	8.3±0.4	**5.4±0.3†**	**6.5±0.7†**	**6.5±0.4†**

n, cell sample size; *N*, mouse sample size; G_{max}, maximum conductance; $V_{1/2(Act)}$, voltage at which 50% of channels are activated; k, slope factor. Data are means ± SEM; **P*<0.05 vs. saline, †*P*<0.05 vs. control, #*P*<0.05 vs. AngII-scramble by two-way repeated measures ANOVA with Holm-Sidak posthoc test.

Table S9: Quantitative PCR primers.

Gene of Interest	Forward Primer (5' → 3')	Reverse Primer (3' → 5')	Amplicon Length
Pde4a	TGGATGCCGTGTTCACAGACCTGG	GTTCTCAAGCACAGACTCATCGTTGTAC	152
Pde4b	CAGGAAAATGGTGATTGACATGGTGTTGG	CGAAGAACCTGTATCCGGTCAGTATAG	152
Pde4d	GGTCATTGACATTGTCCTGGCGACAG	CAGTGCACCATATTCTGAAGGACCTGG	159
Pde3a	GGACAAACCAATTCTTGCTCCAGAACCC	GATACCTGGCTCAGAATACGGCCAC	144
Gapdh	AATGGGGTGAGGCCGGTGCT	CACCCTTCAAGTGGGCCCCG	87